Received: 27 October 2020 | Revised: 19 August 2021 | Accepted: 30 August 2021

DOI: 10.1002/jnr.24967

RESEARCH ARTICLE

JOURNAL OF Neuroscience Research

Light microscopic and heterogeneity analysis of astrocytes in the common marmoset brain

Yorka Muñoz[1] | Francisco Cuevas-Pacheco[2,3] | Gaël Quesseveur[1] | Keith K. Murai[1,4]

[1]Centre for Research in Neuroscience, Department of Neurology & Neurosurgery, Brain Repair and Integrative Neuroscience Program, Research Institute of the McGill University Health Centre, Montreal General Hospital, Montreal, QC, Canada

[2]Department of Mathematics, Universidad Técnica Federico Santa Maria, Valparaiso, Chile

[3]Advanced Center for Electrical and Electronic Engineering, Universidad Técnica Federico Santa Maria, Valparaiso, Chile

[4]Quantitative Life Sciences Graduate Program, McGill University, Montreal, QC, Canada

Correspondence
Keith K. Murai, Centre for Research in Neuroscience, Department of Neurology & Neurosurgery, Brain Repair and Integrative Neuroscience Program, Research Institute of the McGill University Health Centre, Montreal General Hospital, 1650 Cedar Avenue L12-409, Montreal, QC H3G 1A4 Canada.
Email: keith.murai@mcgill.ca

Funding information
Natural Sciences and Engineering Research Council of Canada, Grant/Award Number: 408044-2011 and 69404; International Development Research Centre; Canadian Institutes of Health Research, Grant/Award Number: PJT148569 and 156247; Fonds de recherche du Québec- Santé; National Agency for Research and Development of Chile, Grant/Award Number: 3210453; AC3E Research Group, UTFSM, Grant/Award Number: FB-0008

Abstract

Astrocytes are abundant cells of the central nervous system (CNS) and are involved in processes including synapse formation/function, ion homeostasis, neurotransmitter uptake, and neurovascular coupling. Recent evidence indicates that astrocytes show diverse molecular, structural, and physiological properties within the CNS. This heterogeneity is reflected in differences in astrocyte structure, gene expression, functional properties, and responsiveness to injury/pathological conditions. Deeper investigation of astrocytic heterogeneity is needed to understand how astrocytes are configured to enable diverse roles in the CNS. While much has been learned about astrocytic heterogeneity in rodents, much less is known about astrocytic heterogeneity in the primate brain where astrocytes have greater size and complexity. The common marmoset (*Callithrix jacchus*) is a promising non-human primate model because of similarities between marmosets and humans with respect to genetics, brain anatomy, and cognition/behavior. Here, we investigated the molecular and structural heterogeneity of marmoset astrocytes using an array of astrocytic markers, multi-label confocal microscopy, and quantitative analysis. We used male and female marmosets and found that marmoset astrocytes show differences in expression of astrocytic markers in cortex, hippocampus, and cerebellum. These differences were accompanied by intra-regional variation in expression of markers for glutamate/GABA transporters, and potassium and water channels. Differences in astrocyte structure were also found, along with complex interactions with blood vessels, microglia, and neurons. This study contributes to our knowledge of the cellular and molecular features of marmoset astrocytes and is useful for understanding the complex properties of astrocytes in the primate CNS.

KEYWORDS

astrocytes, cerebellum, confocal imaging, cortex, heterogeneity, hippocampus, marmoset, RRID:AB_10641162, RRID:AB_10673392, RRID:AB_11122614, RRID:AB_141607, RRID:AB_141844, RRID:AB_142581, RRID:AB_162542, RRID:AB_2059853, RRID:AB_2110656, RRID:AB_2194160, RRID:AB_2340472, RRID:AB_2340476, RRID:AB_2340961, RRID:AB_2340962, RRID:AB_2534013, RRID:AB_2534017,

Edited by Christopher Anderson and Cristina Ghiani. Reviewed by Arthur Butt, Yongjie Yang, and Niels Christian Danbolt.

RRID:AB_2534102, RRID:AB_2535792, RRID:AB_2536183, RRID:AB_2620004, RRID:AB_2763902, RRID:AB_297885, RRID:AB_304334, RRID:AB_397474, RRID:AB_476894, RRID:AB_477499, RRID:AB_839504, RRID:AB_90949, statistical analysis

1 | INTRODUCTION

Astrocytes are among the most abundant cells of the central nervous system (CNS) and play critical roles in CNS development, maintenance, and function. Accumulating evidence has demonstrated that astrocytes comprise a surprisingly heterogeneous population of cells in the CNS, with properties that vary depending on their developmental origin, morphology, sensitivity to environmental cues, metabolism, and physiology (Oberheim et al., 2012; Zhang & Barres, 2010). Two main types of astrocytic heterogeneity have been recognized including heterogeneity of astrocytes between brain regions (inter-regional heterogeneity) and heterogeneity of astrocytes within brain regions (intra-regional heterogeneity) (Ben Haim & Rowitch, 2017). Although the impact of such heterogeneity on astrocytic function remains to be fully understood, it does allow astrocytes to have brain region-specific properties (Chai et al., 2017; Corkrum et al., 2019; Khakh & Sofroniew, 2015; Martin-Fernandez et al., 2017) and more optimally control their local microenvironment (Farmer et al., 2016). Recent studies using single-cell mRNA profiling and transcriptomic mapping in rodent brain have distinguished multiple types of protoplasmic astrocytes in the rodent cerebral cortex (Batiuk et al., 2020; Bayraktar et al., 2020). The differential expression of molecules by astrocytes may be important for maintaining healthy brain function and also for controlling the response of astrocytes to CNS injury or disease.

Research using non-human primates has provided valuable insight into brain function and the neural circuits that underlie cognition, sensorimotor integration, and behavior. At the same time, non-human primate research has played an instrumental role in understanding neurological conditions such as Alzheimer's disease, Parkinson's disease, Huntington's disease, autism spectrum disorder, schizophrenia, anxiety, depression, attention deficit hyperactivity disorder, and obsessive–compulsive disorder (Aron Badin, 2018; Li et al., 2019; Oikonomidis et al., 2017; Pignataro et al., 2018; Zhao et al., 2018). The common marmoset (*Callithrix jacchus*) has emerged as a robust model for understanding primate brain organization, function, and behavior. Marmosets share important features with humans with respect to brain anatomy, cognition, complex behavior, and age-related neurological decline (Mattison & Vaughan, 2017; Ross et al., 2012; Tardif, 2019). In comparison to rodents, marmosets have a more complex brain anatomy that enables more detailed investigations of brain organization, function, and molecular/cellular properties (de la Mothe et al., 2006; Mitchell & Leopold, 2015; Roberts et al., 2007; Shimogori et al., 2018). Recent development of genetic engineering approaches is also permitting advanced modeling of brain disorders and diseases in marmosets (Matsuzaki et al., 2018; Park et al., 2016; Sasaki et al., 2009; Sato et al., 2016; Shinohara et al., 2016; VanderVeen et al., 2014). While much has been learned about the properties of neurons and neuronal physiology underlying marmoset behavior, there remains a paucity of information about the properties of astrocytes in marmosets which are among the most abundant and diverse glial cells in the brain (Budoff et al., 2019; Goldshmit & Bourne, 2010; Goldshmit et al., 2014; Honavar & Lantos, 1987; McDermott & Lantos, 1989; Missler et al., 1994; van Luijn et al., 2016; Williams et al., 2005; Yamamoto et al., 2012). Further investigations are needed to understand the complex properties of astrocytes and identify species-specific differences in their organization, structure, and molecular profile.

In this study, we investigated the organization, structure, and molecular properties of astrocytes in the marmoset cortex, hippocampus, and cerebellum using multi-label confocal imaging with a focus on inter-regional and intra-regional molecular and structural differences within this cell population. We identified multiple glial fibrillary acidic protein (GFAP)-expressing astrocyte populations in cerebral cortex including interlaminar (ILA), protoplasmic, and fibrous astrocytes, as described in other monkey species. Cluster analysis was used to more systematically find subpopulations of cortical astrocytes expressing different levels of molecules including the glutamate transporter EAAT2, potassium channel Kir4.1, GABA transporter GAT3, and glutamine synthetase (GS).

Significance

We found that astrocytes in the marmoset brain show inter-regional differences in expression of astrocytic markers in cortex, hippocampus, and cerebellum. We also identified intra-regional variation in expression of markers for glutamate/GABA transporters, and potassium and water channels, showing different subpopulations of astrocytes throughout the cortical and hippocampal parenchyma. Furthermore, we show a strong polarization of astrocytes located on the edge of pyramidal cell layer in the CA1 area of hippocampus and a prominent network of lateral processes of Bergmann glia in the cerebellar cortex. Finally, we show the complex interactions of astrocytes with blood vessels, microglia, and neurons. This study contributes to our knowledge of the cellular and molecular features of marmoset astrocytes and is useful for understanding the complex properties of astrocytes in the primate central nervous system.

In the hippocampus, we found that CA1 astrocytes located on the edge of the pyramidal cell layer show a strong structural polarity. Furthermore, in the cerebellum, we detected lateral appendages/processes that extend from Bergmann glial cell fibers spanning the molecular layer. This study contributes to our knowledge of the cellular and molecular features of marmoset astrocytes and is useful for understanding the complex properties of astrocytes in the primate CNS.

2 | MATERIALS AND METHODS

2.1 | Animals

Experiments were approved by the Montreal General Hospital Facility Animal Care Committee and followed the guidelines of the Canadian Council on Animal Care. Marmosets were housed and cared for according to standard operating procedures at McGill University and the Research Institute of the McGill University Health Centre.

2.2 | Brain and sample preparation

Three marmosets were utilized for this study. One marmoset (male, 1 year and 7 months old) was perfused with phosphate-buffered saline (PBS) followed by 10% formaldehyde. The brain was subsequently collected and post-fixed in 10% formaldehyde for 3 additional days. The brain of a second marmoset (male, 2 years old) was drop fixed in 10% formaldehyde for 3 days. A third marmoset (female, 2 years old) was perfused with PBS followed by 4% formaldehyde and post-fixed for 2 hr. All marmoset brains were cryoprotected in 30% sucrose/PBS solution for 3 days before being embedded in Tissue Tek O.C.T. Compound (Sakura Finetek, USA), frozen, and sectioned coronally (50 μm) with a cryostat. Sections were collected free floating in cryoprotectant solution containing ethylene glycol (30%), and glycerol (30%) in 0.05 M phosphate buffer (PB, pH 7.4) until processed for immunolabeling.

2.3 | Immunolabeling and confocal imaging

Free-floating sections were subjected to immunolabeling procedures as previously described in detail (Quesseveur et al., 2019). Briefly, sections were rinsed three times in Dulbecco's PBS (PBS, Millipore-Sigma, Germany) and irradiated with ultraviolet (UV) light for approximately 16 hr in a biosafety cabinet to reduce autofluorescence of the sections. Sections were then treated with 0.5% Triton X-100/PBS solution for 30 min and blocked in 2% normal horse serum/0.4% Triton X-100/PBS (blocking solution) for 2 hr at room temperature (RT). Triton X-100 and normal horse serum were purchased from Millipore-Sigma (Germany) and Thermo Fisher Scientific (US), respectively. Primary antibodies (Table 1) were applied for 72 hr at indicated dilutions in blocking solution at 4°C. It should be noted that robust specificity controls for the antibodies are not available. The antibodies have been characterized in rodents but have not been validated in marmoset tissues. Peptides and proteins were generally well conserved between the species used to generate the antibody and the marmoset species (Table 2). Moreover, similar labeling in particular astrocytic populations and specific astrocytic compartments (i.e., nucleus, cytoplasm, soma, fine processes, and endfeet) was observed in both rodent and marmoset astrocytes, providing confidence that the signals detected are reliable. Future experiments, for example using gene-knock-out approaches, will be useful in validating the specificity of the antibodies in marmosets. After applying primary antibodies, sections were rinsed three times for 10 min in PBS and then incubated with fluorescent tagged-secondary antibodies in blocking solution for 2 hr at RT (Table 3). Then, slices were incubated with a 1:10,000 solution of 4′,6-diamidino-2-phenylindole (DAPI, Millipore-Sigma, Germany) for 20 min at RT to label nuclei. Sections were rinsed three times in PBS and mounted using SlowFade Gold Antifade Mountant (ThermoFisher Scientific, US). Image acquisition was made with an Olympus FV-1000 confocal laser scanning microscope using 10×, 20×, 40×, and 60× objectives (numerical aperture (NA): 0.30, 0.85, 1.30, and 1.40, respectively). For each label, images were acquired as a stack with at least 14 optical sections. Image analysis was performed with NIH ImageJ software. Only minor differences in immunofluorescence signal were observed between marmoset samples fixed using different methods (See Brain and Sample Preparation section) with the exception of the signal for Connexin 43 (Cx43). Because of this fixation-related inconsistency, Cx43 labeling was not included in detailed analysis (Figures S1–S3).

2.4 | Analysis of astrocyte structural polarity in the hippocampus

To compare astrocytes on the edge of the pyramidal cell layer and astrocytes located in the stratum radiatum (S. radiatum; >100 μm far from the edge of pyramidal layer) at least three images (with four to six astrocytes in each image) were randomly selected from the S. radiatum and edge of the Stratum pyramidale (S. pyramidale). Astrocytes were identified by GFAP labeling and each sample was imaged using a 60× objective (1.4 NA) and *z*-stacks were collected. The length of primary and secondary processes and number of total processes were analyzed using the Simple Neurite Tracer plugin for ImageJ. Measurements were made following maximum projections of *z*-stacks and continuity of the processes was verified by visualizing the 3D image stack. For astrocytes on the edge of the S. pyramidale, we calculate the percentage of total processes orientated apically (processes toward the S. oriens) and basally (processes protruding from the soma toward the S. radiatum) for each astrocyte analyzed. We classified the orientation of astrocytic processes using the following classification bins based on the pyramidal cell layer as

TABLE 1 List of primary antibodies used

Name	Immunogen	Details	Concentration/ working dilution
Anti-GFAP antibody produced in guinea pig	Recombinant protein corresponding to AA 1 to 432 from human GFAP	Synaptic systems, # 173004, polyclonal guinea pig antiserum, RRID:AB_10641162	Not provided/1:500
Anti-S100β antibody produced in mouse	Bovine brain S-100b	Sigma-Aldrich, # S2532, monoclonal antibody, RRID:AB_477499	Not provided/1:500
Anti-GS antibody produced in mouse	Glutamine synthetase purified from sheep brain	Millipore, # MAB302, monoclonal antibody, RRID:AB_2110656	2 μg/ml/1:500
Anti-Sox9 antibody produced in goat	*E. coli*-derived recombinant human SOX9 Met1-Lys151	R&D system, # AF3075, polyclonal antibody, RRID:AB_2194160	4 μg/ml/1:250
Anti-Calbindin (D28K) antibody produced in mouse	Bovine kidney Calbindin-D	Sigma-Aldrich, # C9848, monoclonal antibody, RRID:AB_476894	Not provided/1:250
Anti-EAAT2 antibody produced in guinea pig	Synthetic peptide from the carboxy-terminus of rat GLT-1	Millipore, # AB1783, polyclonal antibody, RRID:AB_90949	Not provided/1:500
Anti-EAAT1[a] antibody produced in rabbit	Synthetic peptide corresponding to Rat EAAT1 (C terminal, 20 residues)	Abcam, # Ab416, polyclonal antibody, RRID:AB_304334	2 μg/ml/1:500
Anti-Kir4.1 antibody produced in guinea pig	Peptide corresponding to AA 356-375 of rat $K_{ir}4.1$	Alomone labs, # AGP-012, polyclonal antibody, RRID:AB_2340962	1.6 μg/ml/1:500
Anti-GAT3 antibody produced in guinea pig	Synthetic peptide corresponding to AA 612 to 627 of mouse GAT3	Synaptic systems, # 274304, polyclonal guinea pig antiserum, RRID:AB_2620004	Not provided/1:500
Anti-AQP4 antibody produced in goat	Peptide mapping at the C-terminus of human AQP4	Santa Cruz Biotechnology, # SC-9888, polyclonal antibody, RRID:AB_2059853	2 μg/ml/1:500 KO validated
Anti-AQP4 antibody produced in rabbit	Peptide corresponding to AA 300-314 of rat AQP4	Alomone lab, # AQP4-014, polyclonal antibody, RRID:AB_11122614	1.6 μg/ml/1:500
Anti-GluA1 antibody produced in guinea pig	Peptide corresponding to AA 271-285 of rat GluR1	Alomone lab, # AGP-009, Polyclonal antibody, RRID:AB_2340961	3.2 μg/ml/1:250
Anti-Cx43 antibody produced in mouse	Peptide corresponding to AA 252-270 of Rat Connexin-43	BD transduction, # 610062, monoclonal antibody, RRID:AB_397474	0.5 μg/ml/1:500
Anti-Lam antibody produced in rabbit	Recombinant fusion protein corresponding to AA 862-1111 of human LAMC2	ABClonal, # A1869, polyclonal antibody, RRID:AB_2763902	Not provided/1:50
Anti-Iba1 antibody produced in rabbit	Synthetic peptide, C-terminal of Iba1	WAKO, # 019-19741, polyclonal antibody, RRID:AB_839504	1 μg/ml/1:500
Anti-MAP2 antibody produced in mouse	HM-2 hybridoma produced from mice immunized with Rat MAP2	Abcam, # Ab11267, monoclonal antibody, RRID:AB_297885	2 μg/ml/1:250
Anti-Kv2.1 antibody produced in mouse	Synthetic peptide AA 837-853, C-terminus of rat Kv2.1	NeuroMAB, # 75014, monoclonal antibody RRID:AB_10673392	3.3 μg/ml/1:300

[a]An antibody tested but not used for the study; See Table 2 for further details.

a reference point: 0°–89°, 90°–179°, 180°–269°, and 270°–359°. We considered apical processes as being orientated between 0°–89° and 270°–359°, and basal processes orientated between 90°–179° and 180°–269°. We used the same system to analyze astrocytes located in the S. radiatum.

2.5 | Astrocyte molecular heterogeneity analysis

To study the variation in expression of astrocytic proteins, a cluster-based method was performed on immunofluorescence images. The calculations were done using R software (version 4.0.1). First, we defined the position of astrocytes in each image using GS as a general marker. Next, we created a circular region-of-interest (ROI) with a 30 μm diameter for each GS+ astrocyte in both cortical and hippocampal images. For each ROI, we computed the empirical distribution function (ECDF) of the pixels inside the region (F_i, for $i = 1, \ldots, N$, where N is the total number of identified astrocytes), and applied a hierarchical cluster algorithm (Kaufman & Rousseeuw, 2009) over the obtained ECDFs. The hierarchical cluster algorithm required two inputs: a distance matrix, D, with elements $D_{ij} = d(F_i, F_j)$, where $d(\cdot,\cdot)$ is a suitable distance function; and a linkage criterion,

TABLE 2 Antibodies used and amino acid conservation between species

Antibody used in the study	Immunizing antigen (peptide or protein) and species	Amino acid (aa) identity conservation with marmoset ortholog	Alignment Orange letters = Conservative replacements Red letters = Non-conservative replacements or absences
EAAT2	Not specified used last 25aa Rat	100% (25 of 25aa)	550 560 570 Rat CKVTLAANGKSADCSVEEEPWKREK Marm CKVTLAANGKSADCSVEEEPWKREK
EAAT1 (omitted from study)	aa 524-543 Rat	80% (16 of 20aa)	530 540 Rat QLIAQDNEPEKPVADSETKM Marm QLIAQDSETEKPI-DSETKM
Kir4.1	aa 356-375 Rat	100% (20 of 20aa)	360 370 Rat KLEESLREQAEKEGSALSVR Marm KLEESLREQAEKEGSALSVR
GAT3	aa 612-627 Mouse	88% (14 of 16aa)	620 Mouse KGDGTISAITEKETHF Marm KSDGTIAAITEKETHF
GluA1	aa 271-285 Rat	80% (12 of 15aa)	280 Rat RTSDSRDHTRVDWKR Marm KNSDARDHTRVDWKR
AQP4 (Human)	Not Specified Used Last 20aa Human	95% (19 of 20aa)	310 320 Human VDRGEEKKGKDQSGEVLSSV Marm IDRGEEKKGKDQSGEVLSSV
AQP4 (Rat)	aa 300-314 Rat	93.3% (14 of 15aa)	300 310 Rat HVIDIDRGDEKKGKD Marm HVIDIDRGEEKKGKD
S100ß	aa 1-92 Bovine	96.7% (89 of 92aa)	10 20 30 Bov MSELEKAVVALIDVFHQYSGREGDKHKLKKSELKELIN Marm MSELEKAMVALIDVFHQYSGREGDKHKLKKSELKELIN 40 50 60 70 Bov NELSHFLEEIKEQEVVDKVMETLDSDGDGECDFQEFMA Marm NELSHFLEEIKEQEVVDKVMETLDNDGDGECDFQEFMA 80 90 Bov FVAMITTACHEFFEHE Marm FVAMVTTACHEFFEHE
SOX9	aa 1-151 Human	100% (151 of 151aa)	10 20 30 Hum MNLLDPFMKMTDEQEKGLSGAPSPTMSEDSAGSPCPSG Marm MNLLDPFMKMTDEQEKGLSGAPSPTMSEDSAGSPCPSG 40 50 60 70 Hum SGSDTENTRPQENTFPKGEPDLKKESEEDKFPVCIREA Marm SGSDTENTRPQENTFPKGEPDLKKESEEDKFPVCIREA 80 90 100 110 Hum VSQVLKGYDWTLVPMPVRVNGSSKNKPHVKRPMNAFMV Marm VSQVLKGYDWTLVPMPVRVNGSSKNKPHVKRPMNAFMV 120 130 140 150 Hum WAQAARRKLADQYPHLHNAELSKTLGKLWRLLNESEK Marm WAQAARRKLADQYPHLHNAELSKTLGKLWRLLNESEK

(Continues)

TABLE 2 (Continued)

Antibody used in the study	Immunizing antigen (peptide or protein) and species	Amino acid (aa) identity conservation with marmoset ortholog	Alignment Orange letters = Conservative replacements Red letters = Non-conservative replacements or absences
GFAP	aa 1-432 Human	98.1% (424 of 432aa)	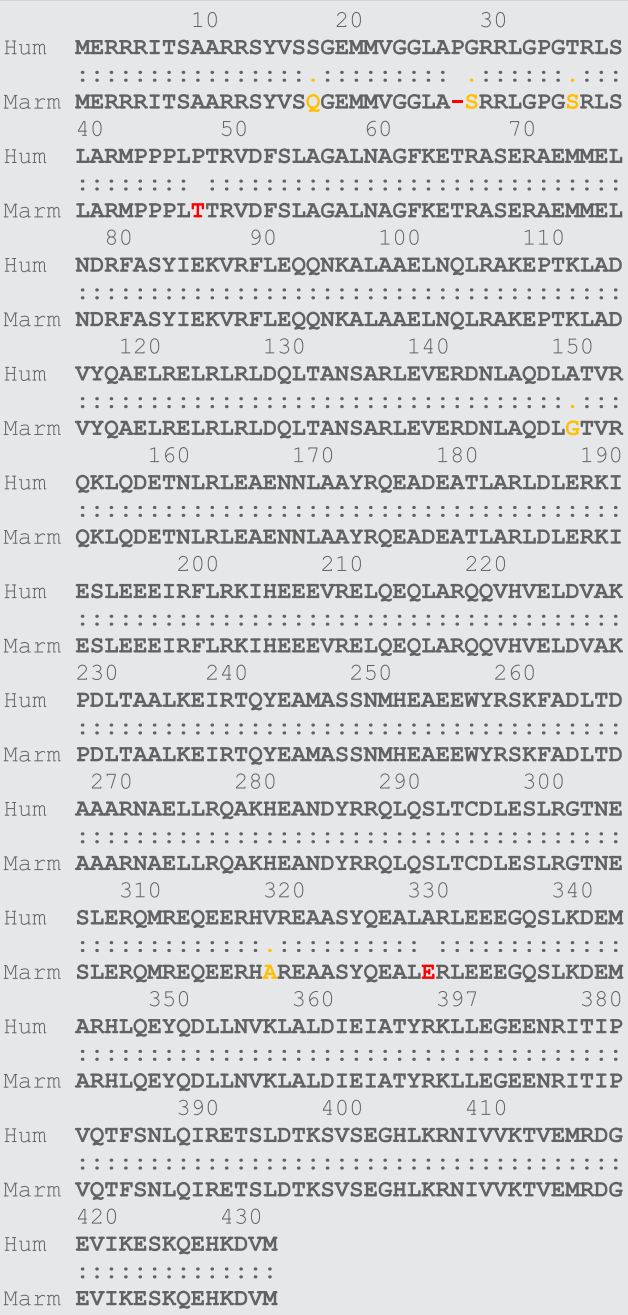

(Continues)

TABLE 2 (Continued)

Antibody used in the study	Immunizing antigen (peptide or protein) and species	Amino acid (aa) identity conservation with marmoset ortholog	Alignment Orange letters = Conservative replacements Red letters = Non-conservative replacements or absences
GS	aa 1-373 Sheep	96% (358 of 373aa)	10 20 30 She MATSASSHLNKGIKQVYMALPQGEKVQAMYIWIDGTGE Marm MTTSASSHLNKGIKQVYMSLPQGEKVQAMYIWIDGTGE 40 50 60 70 She GLRCKTRTLDSEPKCIEELPEWNFDGSSTFQSEGSNSD Marm GLRCKTRTLDSEPKCVEELPEWNFDGSSTLQSEGSNSD 80 90 100 110 She MYLVPAAMFRDPFRKDPNKLVFCEVFKYNRKPAETNLR Marm MYLVPAAMFRDPFRKDPNKLVLCEVFKYNRKPAETNLR 120 130 140 150 She HTCKRIMDMVSNQRPWFGMEQEYTLMGTDGHPFGWPSN Marm HTCKRIMDMVSNQHPWFGMEQEYTLMGTDGHPFGWPSN 160 170 180 190 She GFPGPQGPYYCGVGADKAYGRDIVEAHYRACLYAGIKI Marm GFPGPQGPYYCGVGADRAYGRDIVGAHYRACLYAGVKI 200 210 220 She GGTNAEVMPAQWEFQIGPCEGIDMGDHLWVARFILHRV Marm AGTNAEVMPAQWEFQIGPCEGISMGDHLWVARFILHRV 230 240 250 260 She CEDFGVIATFDPKPIPGNWNGAGCHTNFSTKAMREENG Marm CEDFGVIATFDPKPIPGNWNGAGCHTNFSTKAMREENG 270 280 290 300 She LKYIEEAIEKLSKRHQYHIRAYDPKGGLDNARRLTGFH Marm LKYIEEAIEKLSKRHQYHIRAYDPKGGLDNARRLTGFH 310 320 330 340 She ETSNINDFSAGVANRGASIRIPRTVGQEKKGYFEDRRP Marm ETSNINDFSAGVANRSASIRIPRTVGQEKKGYFEDRRP 350 360 370 She SANCDPFAVTEALIRTCLLNETGDEPFQYKN Marm SANCDPFSVTEALIRTCLLNETGAKPFQYKN

which is selected by the user. For the distance matrix, we used the Kolmogorov–Smirnov (KS) metric (Rachev et al., 2013) given by $d(F_i, F_j) = Max|F_i(x) - F_j(x)|$, where the maximum is taken over $x \in [0, 1]$. To select the linkage criteria, we initially applied four criteria (complete, single, average, and ward2) and compared them using an agglomerative coefficient (Kaufman & Rousseeuw, 2009) (Figure S4) which showed that the Ward2 criteria as the most effective (Miyamoto et al., 2015; Murtagh & Legendre, 2014). The optimal number of clusters was obtained by choosing the integer such that the average silhouette index reaches its first maximum (Rousseeuw, 1987). The results of the cluster analysis and the total number of clusters identified were depicted in dendrograms (Figures 4, 7, S5 and S6, left panel). The code used for this method can be found at http://github.com/FcoCuevas87/AstrocyteClustering.

2.6 | Statistical analysis

Statistical analysis was performed with GraphPad Prism software. At least one hundred measurements were carried out to assess the length of processes of each astrocyte. Data sets were compared using an unpaired Student's two-tailed *t* test and results presented as mean ± standard deviation (*SD*). To determine the orientation of the processes, between 15 and 20 astrocytes were measured and the total number of processes of each astrocyte were considered to calculate the percentage of total processes orientate apically and basally. Data sets were compared using a paired Student's two-tailed *t* test and results presented as mean ± *SD*. A p value of <0.05 was considered statistically significant.

TABLE 3 Listing of secondary antibodies used

Name	Details	Concentration/working solution
Alexa Fluor 488 donkey anti-guinea pig IgG	Jackson ImmunoResearch, # 706-545-148, RRID:AB_2340472	1.5 μg/ml/1:500
Alexa Fluor 647 donkey anti-guinea pig IgG	Jackson ImmunoResearch, # 706-605-148, RRID:AB_2340476	1.5 μg/ml/1:500
Alexa Fluor 488 donkey anti-mouse IgG	Thermo Fischer, # A21202, RRID:AB_141607	4 μg/ml/1:500
Alexa Fluor 568 donkey anti-mouse IgG	Thermo Fischer, # A10037, RRID:AB_2534013	4 μg/ml/1:500
Alexa Fluor 647 donkey anti-mouse IgG	Thermo Fischer, # A31571, RRID:AB_162542	4 μg/ml/1:500
Alexa Fluor 488 donkey anti-rabbit IgG	Thermo Fischer, # A21206, RRID:AB_2535792	4 μg/ml/1:500
Alexa Fluor 568 donkey anti-rabbit IgG	Thermo Fischer, # A10042, RRID:AB_2534017	4 μg/ml/1:500
Alexa Fluor 647 donkey anti-rabbit IgG	Thermo Fischer, # A31573, RRID:AB_2536183	4 μg/ml/1:500
Alexa Fluor 488 donkey anti-goat IgG	Thermo Fischer, # A11055, RRID:AB_2534102	4 μg/ml/1:500
Alexa Fluor 568 donkey anti-goat IgG	Thermo Fischer, # A11057, RRID:AB_142581	4 μg/ml/1:500
Alexa Fluor 647 donkey anti-goat IgG	Thermo Fischer, # A21447, RRID:AB_141844	4 μg/ml/1:500

3 | RESULTS

3.1 | Marmoset astrocytes show inter-regional variation in astrocytic marker expression in cerebral cortex, hippocampus, and cerebellum

Protoplasmic astrocytes in the CNS can be identified based on the expression of specific marker proteins and visualization of their complex morphological features including multiple branches/branchlets, discrete anatomical territories, and association with blood vessels (Benjamin Kacerovsky & Murai, 2016). To characterize protoplasmic astrocytes in different areas of the marmoset brain, we utilized antibodies against proteins known to be expressed by rodent astrocytes including the enzyme GS, the transcription factor Sox9, the intermediate filament GFAP, and the glycoprotein S100β. While GS and Sox9 are considered general markers of astrocytes (Rose et al., 2013; Sun et al., 2017), GFAP is expressed sporadically in CNS astrocytic populations and detected in neuronal progenitors (Liu et al., 2010; Yang & Wang, 2015). S100β is also expressed by mature astrocytes (Raponi et al., 2007) as well as and other CNS cells including oligodendrocytes and ependymal cells (Steiner et al., 2007). We focused our analysis on the marmoset cerebral cortex, hippocampus, and cerebellum to provide a better understanding of the cortical and non-cortical distribution and properties of protoplasmic astrocytes. Multi-label analysis was applied to investigate inter- and intra-regional variation of astrocytic marker expression.

3.1.1 | Protoplasmic astrocytes in the cerebral cortex

In primates, the neocortex has undergone an evolutionary expansion leading to its elaborate organization. Unlike other primate species such as macaques and humans, the common marmoset brain is lissencephalic with a more simplified architecture (Homman-Ludiye & Bourne, 2017; Mashiko et al., 2012). Similar to other species, the common marmoset cerebral cortex is divided into six main layers which can be used as reference points to examine the position of astrocytes and understand intra-regional variations in marker expression and structure of astrocytes.

Expression of general astrocytic markers: GS, Sox9, and S100β

To identify protoplasmic astrocytes, we used antibodies against GS, an ATP-dependent enzyme that enables glutamate–glutamine cycling following synaptic transmission through the conversion of L-glutamate into glutamine in astrocytes (Rose et al., 2013). GS is broadly expressed by astrocytes in different brain regions and is considered a general astrocyte marker in the rodent brain (Derouiche & Frotscher, 1991; Norenberg, 1979). In the marmoset cortex, GS was widely expressed by astrocytes and detected in all cortical layers (Figure 1A). At the subcellular level, GS was detected in the cytoplasm and main astrocytic branches with lower signal in fine processes (Figure 1A,a′). Interestingly, in some astrocytes in layer I, GS signal was confined to cell bodies and large branches, with weak expression in smaller branches/branchlets. In layers II–VI, the GS signal was generally high in the cell body and thick branches of astrocytes with variable expression in finer branches, sometimes delineating anatomical boundaries of individual astrocytes and creating a patchy pattern within the neuropil (Figure 1A). To investigate the completeness of detection of the astrocyte population with anti-GS, we co-labeled for Sox9, a transcription factor involved in development and a nuclear marker of astrocytes (Sun et al., 2017). Sox9 labeling was observed in the nuclei of astrocytes throughout cortical layers as well as in nuclei of cells located in the pia mater, suggestive of expression in the glia limitans (Figure 1B). We found that the vast majority of GS-positive cells were Sox9 positive. We also labeled for the secreted glycoprotein S100β which is known to be prevalent in CNS astrocytes. Like GS and Sox9, S100β was found in all cortical layers, being moderately expressed in the cytoplasm and processes of astrocytes (Figure 1C). S100β signal was variable, with patchy expression caused by large areas of lower S100β

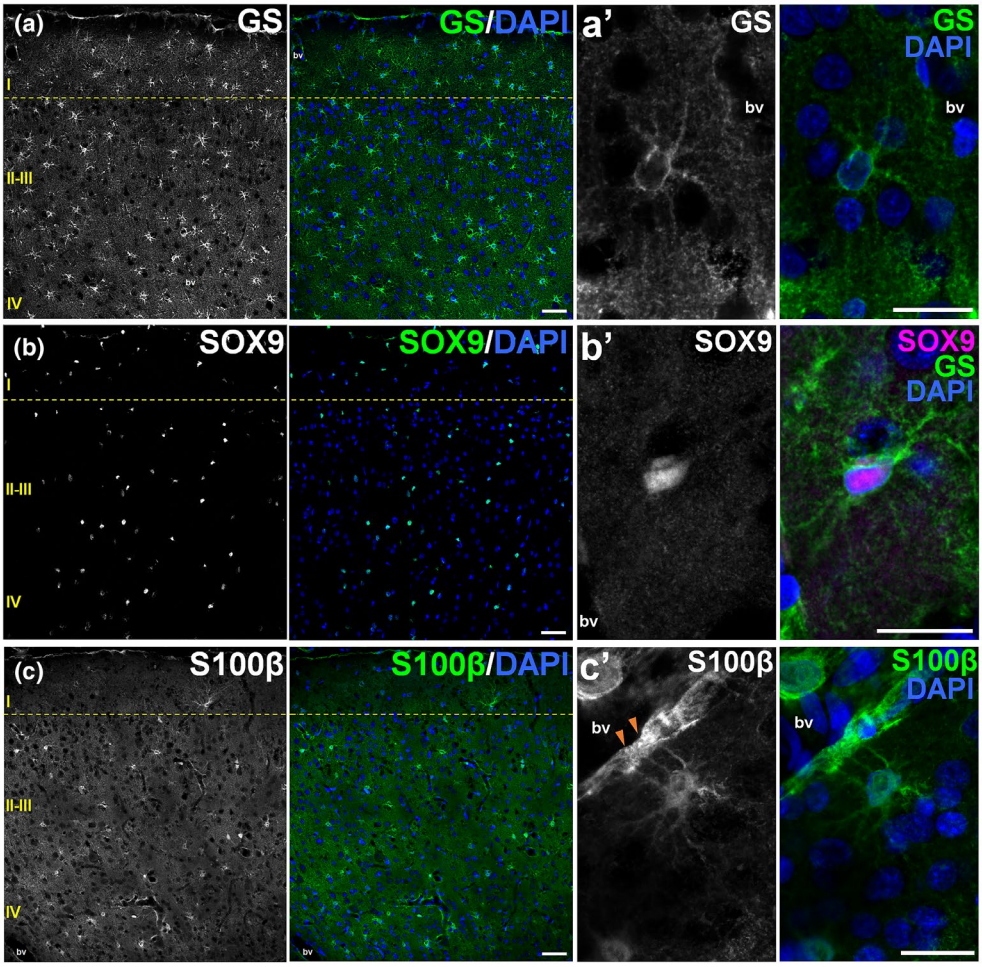

FIGURE 1 Expression of astrocytic markers GS, Sox9, and S100β in the marmoset cerebral cortex. Labeling of coronal sections of marmoset temporal cortex with antibodies against GS (A), Sox9 (B), and S100β (C). Each immunolabeling is contrasted with DAPI staining in the second panel (blue staining). Right panels with lowercase letters (a′–c′) provide a representative view of a single cell labeling. Orange arrowheads show S100β labeling in an astrocytic endfoot in c′. Roman numerals at the left side of panels indicate approximate location of cortical layers. Scale bars: 50 μm in A–C and 20 μm in a′–c′. bv, blood vessel

abundance. Endfeet of some astrocytes showed high levels of S100β (Figure 1C,c′). Thus, GS, Sox9, and S100β are efficient general markers for astrocytes in the cerebral cortex with some variation in the intensity of their expression, especially for S100β.

GFAP labels cortical astrocyte subsets including complex interlaminar astrocytes

GFAP is often thought to be a general marker for astrocytes but in fact shows sparse expression in astrocytes in many regions of the mature CNS. GFAP is also expressed by progenitor cells located in neurogenic niches (Liu et al., 2010; Namba et al., 2005). At least four major morphologic subclasses of GFAP-positive astrocytes have been identified in the adult human temporal cortex and classified as interlaminar astrocytes, protoplasmic astrocytes, varicose projection astrocytes, and fibrous astrocytes (Oberheim et al., 2009). In the marmoset cortex, we identified three major GFAP-positive astrocyte subtypes: Protoplasmic astrocytes, interlaminar astrocytes (divided into pial and subpial subtypes), and fibrous astrocytes (located in white matter area) (Figure 2A–E). To our knowledge, varicose projection astrocytes have only been found in chimpanzee and human brain and have not been identified in other primates including rhesus macaque or squirrel monkeys (Oberheim et al., 2009). Marmoset protoplasmic astrocytes labeled by anti-GFAP were sparsely detected throughout cortical layers II–VI and showed a filamentous pattern of labeling revealed by thick processes leading to branched, smaller processes. GFAP labeling in some astrocytes was also found to project toward and around blood vessels in endfeet (Figure 2C). The endfoot, a specialized astrocytic structure which surrounds blood vessels, was identified by AQP4 expression which was enriched in the endfoot membrane. Fibrous astrocytes labeled by GFAP were frequent in the white matter and showed long, thick, and mostly unbranched primary processes (Figure 2E).

In contrast to the sparse GFAP labeling in astrocytes in layers II–VI, GFAP labeling in astrocytes was particularly enriched in layer I of the marmoset cerebral cortex. GFAP-positive astrocytes in layer I displayed known characteristics of interlaminar astrocytes (ILAs) containing a stellate morphology and extension of long, unbranched processes several micrometers into cortical layers II–III

(Figure 2A). Interlaminar astrocytes have been previously characterized in monkey (*Cebus apella*, *Saimiri sciureus*, *Papio hamadryas*, and *Macaca mulatta*) and human brain (Colombo et al., 1995, 2000; Oberheim et al., 2009) using anti-GFAP. Two distinct types of ILA astrocytes in marsupial and placental mammalians have been described (Falcone et al., 2019): Pial and subpial ILAs. These ILA subtypes differ with respect to their morphology and position in layer I. They also can be classified as "typical" or "rudimentary" depending on whether their GFAP-positive processes exit layer I or not, respectively. We found that the marmoset cortex contained numerous "typical" pial ILAs (Figure 2F–J). These astrocytes showed an inverted pyramidal-shaped soma juxtaposed to the pial surface that is connected to several primary processes (approximately 4 to 6) from the apex of the pyramidal cell body and processes from other portions of the soma (Figure 2F–G). The proximal portion of pial ILA processes appeared thicker than distal portions, running perpendicular or tangential to the pial surface. Pial GFAP-positive ILAs showed colocalization with general markers S100β (Figure 2F), GS (Figure 2G), Sox9 (Figure 2H), and colocalization with other astrocytic proteins including the inwardly rectifying potassium channel Kir4.1 (Figure 2I). AQP4-labeled endfeet traversing the pial surface were not associated with GFAP-labeled pial ILAs (Figure 2J). In contrast to pial ILAs, the somas of subpial ILA were not in contact with the pial surface. Marmoset subpial ILAs displayed a stellate shape with numerous branches (5–15 processes) (Figure 2K–L). Some branches reached to the pial surface and other processes show seemingly random orientation. One or two interlaminar processes from subpial ILAs were found to penetrate deeper cortical layers (II-IV). These processes projected at perpendicular or oblique angles to the pial surface, could be seen as straight or wavy, and finished in varicosities or bulb-like structures (Colombo et al., 1997). In general, only one interlaminar process running mostly to layer II–III was detected for each subpial ILA (Figure 2B, orange arrowheads), with the thickest part of the process being proximal to the cell body. Subpial GFAP-positive ILAs also showed colocalization with the markers S100β (Figure 2K), GS (Figure 2L), Sox9 (Figure 2M), and colocalization with astrocytic protein Kir4.1 (Figure 2N). Subpial ILAs projected toward blood vessels and endfeet labeled by AQP4. Large AQP4-positive punctate was also detected in primary and some secondary branches of subpial ILAs (Figure 2O, orange arrowheads). Marmoset ILA processes did not show the extreme tortuosity which is characteristic in ILAs identified in ape and human brain (Oberheim et al., 2009).

Expression of glutamate and GABA transporters and Kir4.1 in cortical astrocytes

Astrocytes play a critical role in reuptake and recycling of neurotransmitters and ions. In particular, astrocytes are the main cell type expressing the glutamate transporters EAAT2/SLC1A2/GLT-1 (now referred to as EAAT2) and EAAT1/SLC1A3/GLAST (now referred to as EAAT1) (Chaudhry et al., 1995), as well as the GABA transporter GAT3/SLC6A11 (now referred to as GAT3) (Minelli et al., 1996). They also abundantly express the inward rectifying potassium channel Kir4.1 (Higashi et al., 2001). In the marmoset cortex, EAAT2 showed intra-regional variation in its expression. Notably, EAAT2 was low to undetectable in the superficial portion of cortical layer I and correlated with the low expression of GS in fine processes of astrocytes in cortical layer I. This pattern of EAAT2 localization strongly differed from the high and often patchy expression of EAAT2 in layers II–IV (Figure 1A and Figure 3A). Interestingly, EAAT2 showed very low expression near some blood vessels (Figure 3A). The GABA transporter GAT3 showed low to moderate expression on astrocytes throughout layers I–VI. GAT3 also showed variable expression around blood vessels (Figure 3B). Consistent with their function in potassium homeostasis, cortical astrocytes also expressed Kir4.1. Kir4.1 displayed heterogeneous expression in cortical layers with particularly high expression in layers II/III and lower expression in layer IV. Like for EAAT2 and GAT3, Kir4.1 showed variable expression around blood vessels (Figure 3C). Thus, neurotransmitter transporters and ion channels showed differential expression across cortical layers.

Heterogeneity analysis of astrocytic protein expression in cortex

To better understand the variable expression of astrocytic proteins in cortex, we developed a method to: (a) identify discrete clusters of astrocytes that show similar levels of astrocytic protein expression, and (b) map the position of each astrocyte onto images to map the spatial organization of astrocytes belonging to a specific cluster. To do so, we first defined the position of individual astrocytes in each image using GS which is a suitable general astrocytic marker (Figure 1). We then created a region-of-interest (ROI) for each GS+ astrocyte and computed the empirical distribution function (ECDF) of the pixels inside the ROI. A hierarchical cluster algorithm was applied to identify discrete astrocytic clusters over the obtained ECDFs (Kaufman & Rousseeuw, 2009). Individual astrocytes within clusters were mapped back to their respective images to identify the location of each astrocyte within a cluster. Using this method, we found that labeling for EAAT2 (Figure 4A) led to identification of three clusters of astrocytes that showed similar levels of expression. For EAAT2, two main clusters appeared along with a minor cluster representing just 6.3% of total cells (Figure 4a′). Astrocytes within EAAT2 clusters tended to group together (Figure 4A). Analysis of GAT3 (Figure 4B) and GS (Figure S5) showed two, rather equally sized clusters of astrocytes (Figures 4B,b′ and S5a′). Astrocytes within GAT3 clusters grouped together while astrocytes within GS clusters appeared more generally dispersed. Interestingly, astrocytes expressing Kir4.1 segregated into three main clusters, and consistent with our previous observations (Figure 3C), Kir4.1 showed a more stratified organization of Kir4.1-expressing astrocytes (Figure 4C,c,c′). Thus, astrocytes show substantial variation in the expression of specific proteins in cortex. This variation can be used to identify discrete clusters of astrocytes and allow cross-referencing of protein expression to their position within cortex.

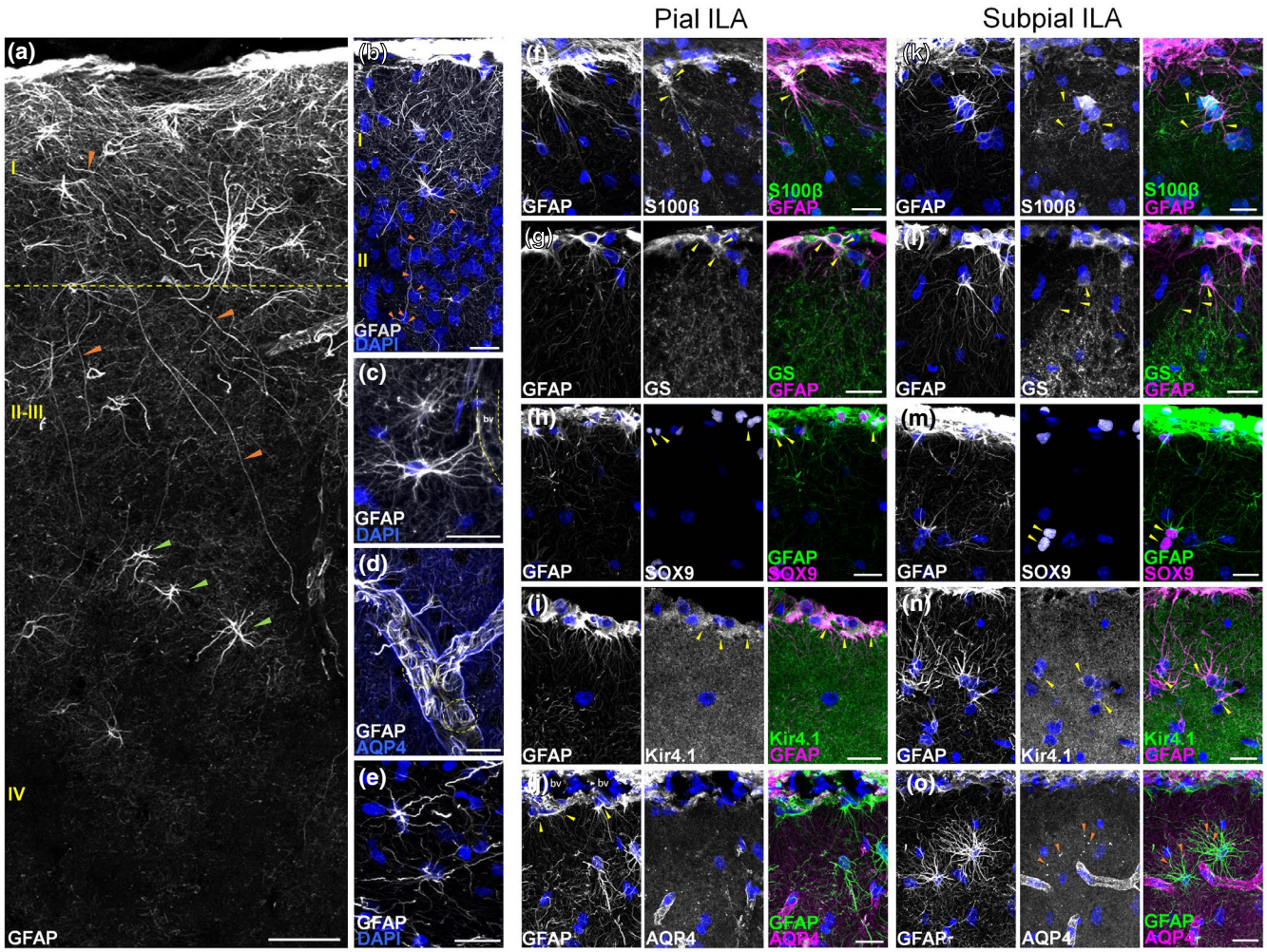

FIGURE 2 GFAP labels marmoset cortical astrocytic populations including complex interlaminar astrocytes. (A–E) Sparsely labeled GFAP-positive astrocytes across cortical layers. The approximate location of cortical layers indicated by Roman numerals I to IV (yellow). Orange arrowheads show interlaminar processes and green arrowheads define protoplasmic astrocytes (A). Detailed images of an interlaminar astrocyte (B), protoplasmic astrocyte (C), astrocytic endfeet (D), and white matter astrocytes (E). DAPI (blue) is used as a nuclear marker and AQP4 (blue) as an endfoot marker. Scale bar: 50 μm (A), 20 μm (B, C, and E), and 5 μm (D). Subtypes of interlaminar astrocytes (ILA). Marmoset pial ILAs (F–J) and subpial ILAs (K–O) labeled by S100β (F, K), GS (G, L), Sox9 (H, M) and specific astrocytic markers such as Kir4.1 (I, N) and AQP4 (J, O). Yellow arrowheads show astrocytic soma and processes in F–O. Orange arrowheads describe a punctate AQP4 staining. Scale bars: 20 μm (F–O)

3.1.2 | Protoplasmic astrocytes in the hippocampus

The hippocampus is an important brain structure for encoding and consolidating memories (Lisman et al., 2017) and astrocytes are known to play an important role in regulating hippocampal circuits and modulating learning/memory processes (Santello et al., 2019; Singh & Abraham, 2017). The anatomical organization of the marmoset hippocampus resembles that of the human hippocampus showing an S-shaped structure in the ventral-temporal region of the marmoset brain (Figure 5H). As with other species, the marmoset hippocampus contains a densely packed layer of neurons separated into Cornu ammonis 1–3 (CA1, CA2, and CA3), dentate gyrus, and subicular regions. Each CA region is divided into Stratum oriens (S. oriens), Stratum pyramidale (S. pyramidale), and Stratum radiatum (S. radiatum) layers. Here we analyzed astrocytes in area CA1, focusing on their distribution, marker expression, and unique structural features.

Expression of astrocytic markers in area CA1

As in the cerebral cortex, GS was abundantly expressed in astrocytes in all CA1 hippocampal layers. High GS signal was observed in the cell body and main astrocytic branches. Imaging at higher magnification exposed finer processes of protoplasmic astrocytes (Figure 5A, inset). In the S. radiatum, GS-positive astrocytes generally showed round-shaped cell bodies with astrocytic processes orientated radially in a stellate pattern. In contrast, GS-expressing astrocytes in the S. oriens presented more elongated cell bodies with an intricate tree-like arborization containing thick, long primary and secondary branches (Figure 5A). Similar to GS labeling, Sox9 signal was broadly observed in astrocytes in all hippocampal layers (Figure 5B).

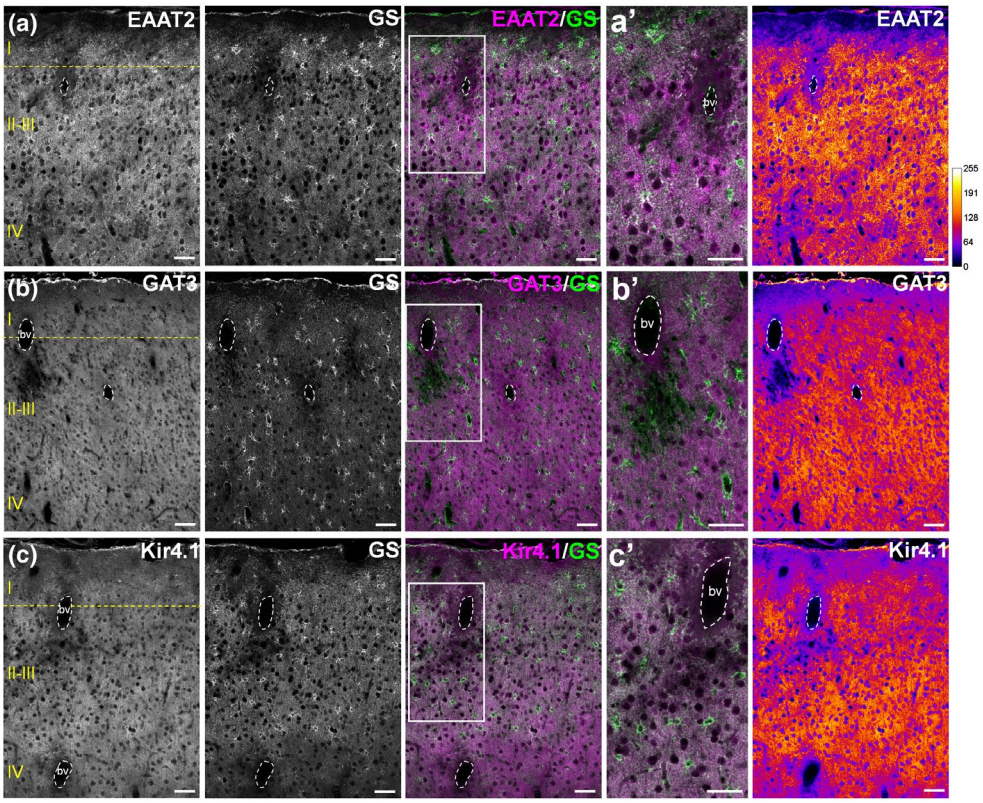

FIGURE 3 Expression of glutamate and GABA transporters, and the potassium channel Kir4.1 in the marmoset cerebral cortex. Double immunostaining of excitatory amino acid transport 2 (EAAT2) and GS (A), GABA transporter 3 (GAT3) and GS (B) and inward rectifier-type potassium channel Kir4.1 and GS (C) in coronal sections from marmoset temporal cortex. GS was used as a counter-label due to its more homogenous distribution in cortical layers. a′–c′ show higher magnifications of white rectangle areas of merged images. Right panels show a heat map of each specific marker showing its expression density through cortical layers. Purple-to-blue color indicates lower intensity signal, while the red-to-yellow color means higher intensity signal. Scale bars: 50 μm in A–C and 20 μm in a′–c′. bv, blood vessel

In contrast, S100β signal in different layers of hippocampus tended to show a patchy pattern and it was generally detected in lower amounts when compared with GS labeling (Figure 5C). S100β signal was concentrated mostly in cell bodies except in S. oriens where it was possible to identify round cell bodies with primary astrocytic processes orientated in all directions (Figure 5C, S. oriens). Similar to the rodent brain, astrocytes in the marmoset hippocampus more strongly and broadly expressed GFAP (Figure 5D) with high expression in astrocytes in S. radiatum and S. pyramidale. In the S. radiatum, astrocytes generally showed round-shaped cell bodies with long and thick astrocytic processes orientated radially in a stellate pattern consistent with the morphology of astrocytes described by GS labeling (Figure 5A). In the S. oriens, sparse astrocytes with cell bodies located in this layer expressed lower levels of GFAP (Figure 5D, S. oriens). We performed double labeling experiments to help correspond markers within the layers. We found a high correspondence of Sox9 and GS labels in all layers (Figure 5E). Furthermore, GFAP and GS showed high correspondence in the S. radiatum and pyramidale with more limited overlap in the S. oriens (Figure 5F). GFAP and S100β had strong correspondence in primary astrocytic processes in most of astrocytes across layers (Figure 5G). Thus, labeling for GS, Sox9, and S100β efficiently labeled the general distribution of hippocampal astrocytes in CA1 layers with some patchy labeling present (i.e., S100β). In contrast, GFAP was strongly expressed in S. radiatum and S. pyramidal astrocytes, but more weakly labeled astrocytes positioned in the S. oriens.

CA1 astrocytes located on the edge of pyramidal cell layer show structural polarity

Remarkably, astrocytes located at the interface of the CA1 S. radiatum and S. pyramidale showed a unique morphology. This was most apparent when labeling for GFAP where these cells extended long, often unbranched processes that traversed the pyramidal cell layer toward the S. oriens (Figure 5I). The morphology of these cells contrasted that of astrocytes in the S. radiatum (Figure 5J) or those in the hilus of the dentate gyrus that lacked consistent orientation (Figure 5K). Three-dimensional morphometry of the GFAP signal was used to measure the degree of polarization of processes from these astrocytes. We found that 67.7 ± 6.8% (average ± *SD*) of total processes from the astrocytes at the edge of the pyramidal cell layer were orientated apically toward the S. oriens and only 32.3 ± 6.8% of processes had a basal orientation toward the S. radiatum (Figure 5L; $p < 0.001$). This differed from astrocytes located within the S. radiatum which showed

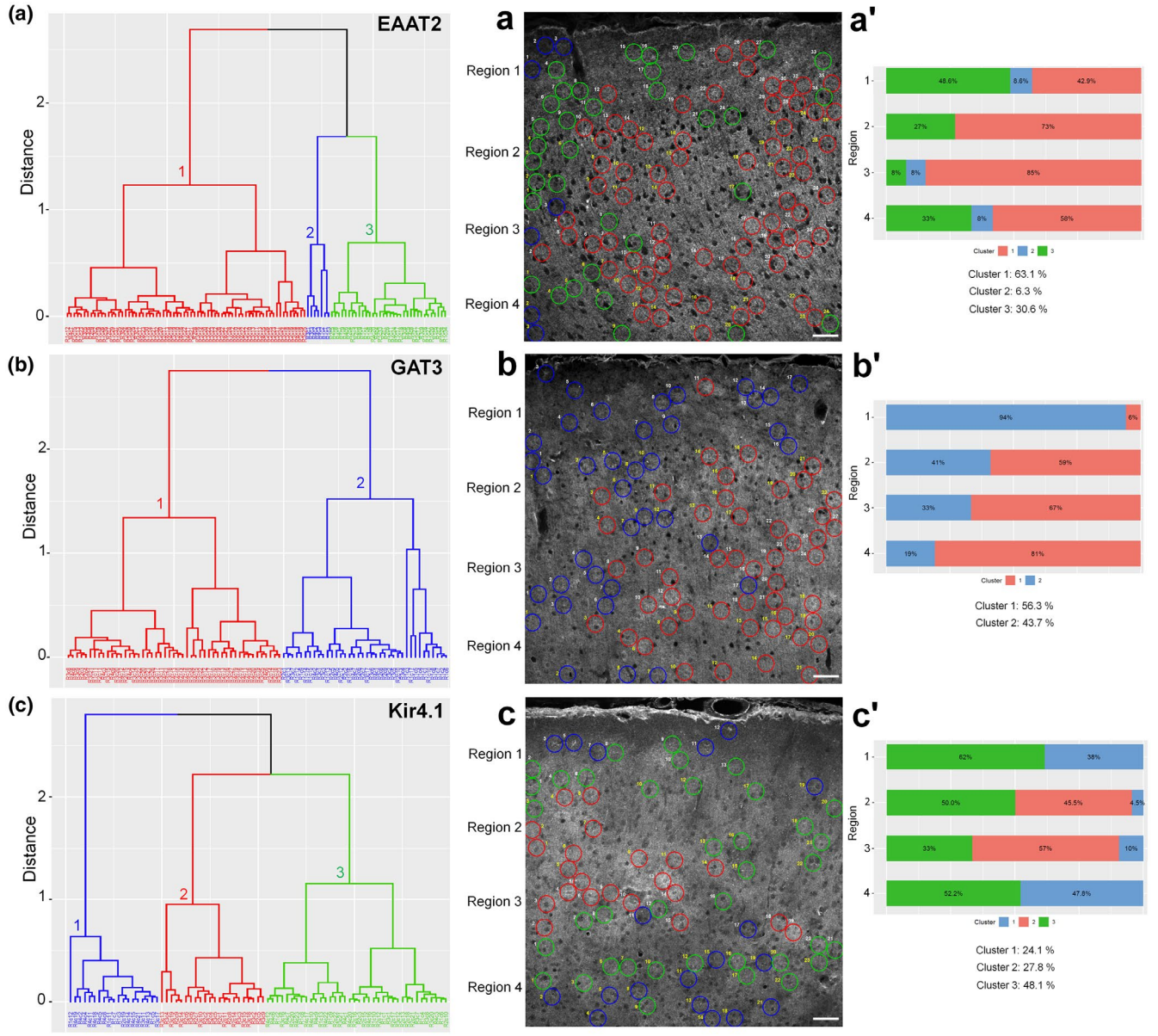

FIGURE 4 Heterogeneity of cortical astrocytes. Hierarchical clustering algorithm identified astrocytic clusters based on the KS distance displayed in the dendrogram (left panel on each row) for EAAT2 (A), GAT3 (B), and Kir4.1 (C). Distance measurements reveal significant separation of astrocytes into distinct clusters. Three different images from two different animals were analyzed for each marker. The spatial organization of astrocytes within clusters is represented a, b, and c. Each astrocyte was identified using GS expression and it was assigned to a region from the pial surface (Region 1, R1) to inner cortical layers (R2, R3, and R4). Scale bars: 50 μm. Each astrocyte was identified with a number, R1 and R3 numbers are indicated in white and R2 and R4 numbers indicated in yellow. Analysis of GS can be found in Figure S5. Every cluster was identified by a number and particular color and the percentage of cells in each cluster in regions 1–4 is shown in a′–c′

44.7 ± 10.3% processes orientated apically and 55.3 ± 10.3% processes orientated basally (Figure 5M; $p = 0.033$). We also analyzed the length of the primary and secondary processes emerging from these polarized astrocytes. We found that the summed length of the apical processes was 82.3 ± 21.5 μm (average ± *SD*) compared with 24.6 ± 10.9 μm of processes orientated basally (Figure 5L; $p < 0.001$). For astrocytes located in the S. radiatum, the summed length of processes was equivalent between apical (36.5 ± 13.5 μm) and basal (39.1 ± 13.9 μm) processes (Figure 5M; not significant). Thus, astrocytes at the interface of the S. radiatum and S. pyramidal showed a specialized, polarized morphology with elongated process that span the pyramidal cell layer and project into the S. oriens.

Expression of glutamate and GABA transporters, Kir4.1 and AQP4 in hippocampus

In contrast to the cerebral cortex, EAAT2 showed more obvious differential expression in the hippocampus. EAAT2 was fairly broadly

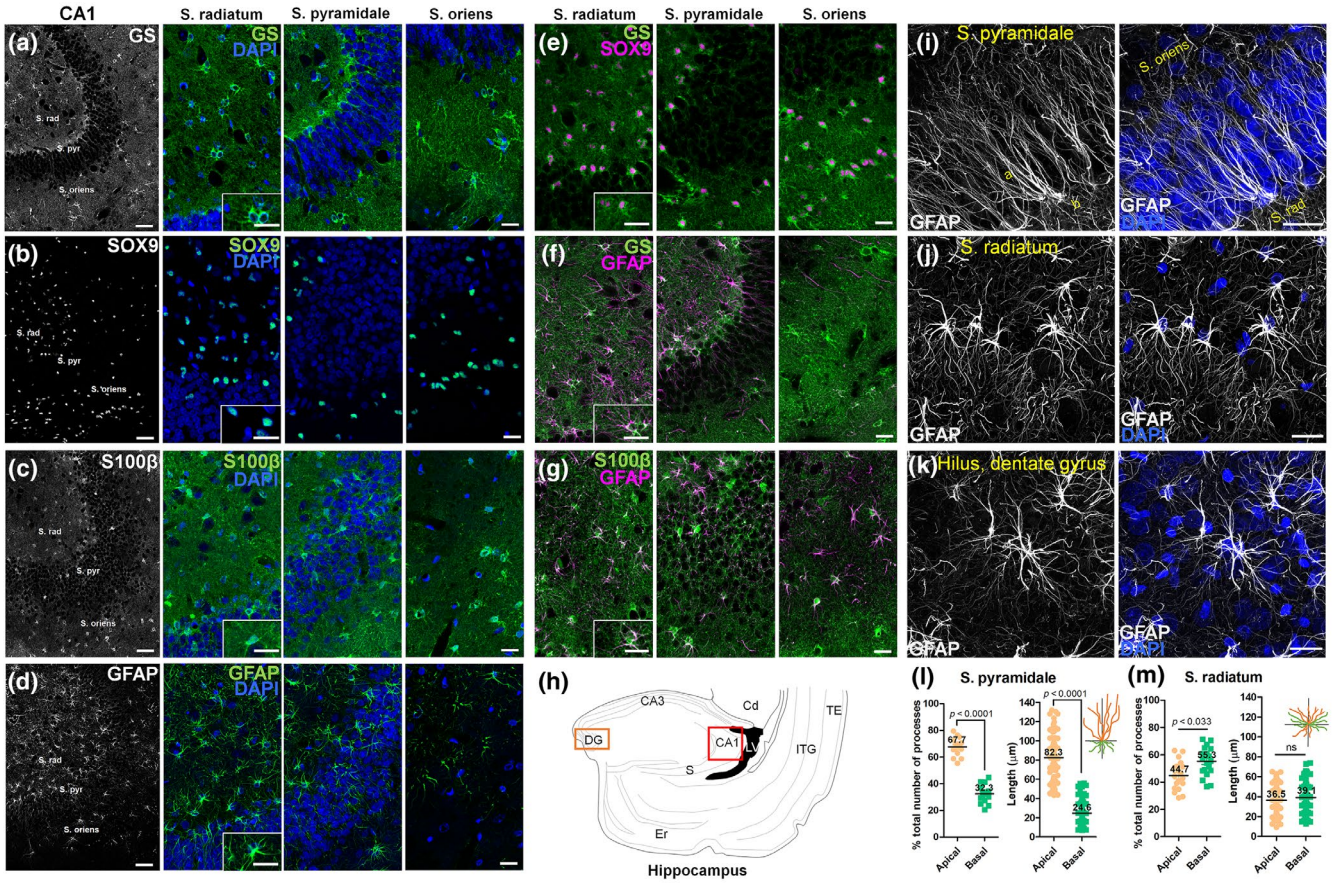

FIGURE 5 Expression of astrocytic markers in the marmoset hippocampus. Labeling of coronal sections of marmoset hippocampus with antibodies against GS (A), Sox9 (B), S100β (C), and GFAP (D). Scale bars: 50 μm. Right insets show a higher magnification of different areas of hippocampus: Stratum radiatum (S. rad), Stratum pyramidale (S. pyr), and Stratum oriens, scale bars: 20 μm. White rectangle areas show higher magnification images, scale bars: 20 μm. Each label is contrasted with DAPI nuclear staining (blue). Double immunostaining of GS and Sox9 (E), GS and GFAP (F), and S100β and GFAP (G) shows heterogeneity. Scale bars: 20 μm. Schematic diagram of the marmoset hippocampus (H) adapted from (Yuasa et al., 2010). CA1, field of CA1 of hippocampus; CA3, field of CA3 of hippocampus; Cd, caudate nucleus; DG, dentate gyrus; Er, entorhinal cortex; ITG, inferotemporal gyrus; LV, lateral ventricle; S, subiculum; TE, temporal cortex. Images detailed from astrocytic processes of astrocytes located at: the border of S. pyramidale (I)—apical processes (a), basal processes (b), S. radiatum (J), and hilus in dentate gyrus (K). Scale bars: 20 μm. (L–M) Degree of structural polarization of astrocytes in S. pyramidale and S. radiatum measured by percentage of total number of processes and quantification of length of astrocytic processes of astrocytes shown in I and J

expressed but was especially enriched in astrocytic processes located at the edge of S. radiatum near the S. pyramidale (Figure 6A). Like EAAT2, GAT3 was enriched in astrocytic processes at the edge of the S. pyramidale with some areas of low expression in the S. radiatum and S. oriens (Figure 6B). Kir4.1 was enriched in a thin layer at the edge of S. pyramidale and showed patchy expression in the S. oriens (Figure 6C). Interestingly, the water channel Aquaporin 4 (AQP4) which contributes to cellular water balance, was abundantly found in the processes of astrocytes in the S. radiatum and within the S. pyramidale with lower overall expression in the S. oriens (Figure 6D). It was consistently detected in astrocytic endfeet surrounding blood vessels.

Heterogeneity analysis of astrocytic protein expression in hippocampus

Applying our method to analyze the variation in protein expression showed the organization of astrocytes with differential expression of particular proteins within the hippocampus. GFAP and AQP4 showed two main clusters of astrocytes with a similar pattern of organization, having a large number of astrocytes from one cluster accumulated at the interface of the S. radiatum and S. oriens (Figure 7A,a,a′,B,b,b′, cluster 1). The remaining astrocytes were dispersed with the S. radiatum and S. oriens (cluster 2). For GAT3, two clusters were identified with most astrocytes in one cluster in the S. radiatum and S. pyramidale (cluster 2), and astrocytes in the other cluster mainly in the S. oriens with only sparse astrocytes in S. radiatum (Figure S6B,b,b′). Analysis of EAAT2 and GS showed three main clusters, with the majority of astrocytes within one cluster amassed at the interface of the S. radiatum and S. oriens (cluster 3), and generally surrounded by astrocytes of the other clusters (Figure S6A,a,a′,C,c,c′). Analysis of Kir4.1 revealed five clusters, with a cluster of astrocytes showing high expression located in the S. oriens (Figure 7C, cluster 1) and two

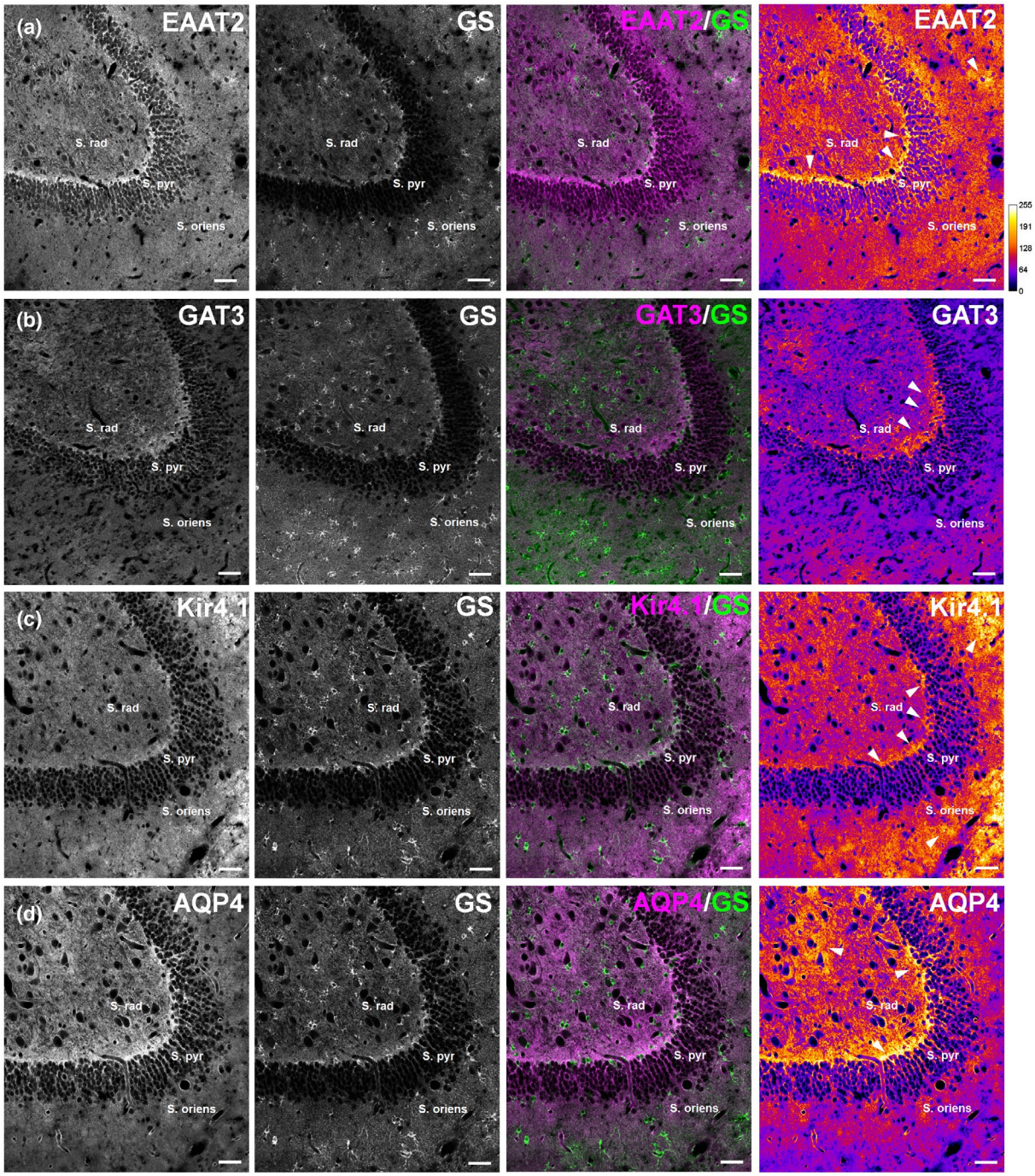

FIGURE 6 Expression of glutamate and GABA transporters, Kir4.1, and AQP4 in the marmoset hippocampus. Labeling of coronal sections of marmoset hippocampus with astrocytic markers associated with subpopulations of astrocytes. Double immunolabeling of EAAT2 and GS (A), GAT3 and GS (B), Kir4.1 and GS (C) and water channel Aquaporin 4 (AQP4) and GS (D). The third panel of each row shows a merged image and the fourth panel is a heat map showing the density of expression of each specific marker. A purple–blue color indicates lower intensity signal and red–yellow color means higher intensity signal. White arrows highlight areas of particularly high signal intensity. Scale bars: 50 μm

clusters showing low expression (Figure 7C,c,c′, clusters 4 and 5). The rest of the astrocytes grouped together within the S. radiatum and S. pyramidale in two different clusters of high and moderate intensity (Figure 7C,c,c′, clusters 2 and 3). Thus, the variable expression of proteins within hippocampal astrocytes can be used to identify specific clusters of cells showing similar levels of expression. Moreover, some of these astrocytic clusters show similar patterns of organization (i.e., GFAP with AQP4 and EAAT2 with GS), while others show more unique organization within the CA1 subfield (i.e., astrocytes with Kir4.1).

3.1.3 | Marmoset cerebellar cortex astrocytes

The cerebellar cortex is composed of a three-layered structure that includes the molecular layer (ML), Purkinje cell layer (PCL), and granular cell layer (GCL) and contains two main astrocyte populations called Bergmann glia (BG) and velate astrocytes (VA), respectively. Fibrous astrocytes are also found in the cerebellar white matter. BG are specialized, polarized astrocytes with cell bodies located in the PCL that project long processes to the pial surface and wrap Purkinje cells dendrites and synapses in the ML (Chan-Palay & Palay, 1974; Reichenbach & Wolburg, 2005). VAs are located in the GCL and contain rounded cell bodies with thin, long, veil-like processes that wrap granule cells, synapses, and help segregate mossy fiber glomeruli (Jakab & Hamori, 1988). Fibrous astrocytes in the white matter have small cell bodies and their processes align with myelinated fibers resulting in an elongated appearance (Reichenbach & Wolburg, 2005).

Expression of astrocytic markers in cerebellar cortex

In the marmoset cerebellum, GFAP was broadly expressed in BG, VA, and white matter astrocytic populations with their processes interdigitating within the PCL/ML, GCL, and white matter, respectively (Figure 8A). In BG, GFAP labeling revealed their characteristic radial processes projecting from the PCL to the pial surface. VA and white matter astrocytes also showed abundant GFAP expression that clearly defined major processes of these cells (Figure 8a,a′). In contrast to GFAP, the expression of S100β, GS, and Sox9 was more variable (Figure 8B–D). S100β showed its highest expression in BG cell bodies within the PCL, pial surface and BG radial processes within the ML while VAs and white matter showed little expression (Figure 8b,b′, BG, VA, WM). In contrast to the selective expression of S100β in BG, GS was detected in multiple astrocyte types with moderate and high expression in the PCL, ML, GCL, and white matter (Figure 8C). BG cell bodies and ascending BG processes in the ML expressed moderate to high levels of GS (Figure 8c,c′, BG). Closer inspection of GFAP, S100β, and GS-expressing BG revealed an intricate pattern of lateral appendages of BG which are oriented perpendicular to the main BG radial fiber in the ML (Figure 8a,a′,b,b′,c,c′, BG, white arrows). In the GCL, moderate GS labeling created a honeycomb-like appearance defined by labeled VA processes surrounding granule cell bodies (Figure 8c,c′, VA). Sox9 showed high expression in BG nuclei surrounding calbindin-positive Purkinje cells (Figure 8D). VAs and white matter astrocytes showed mainly low to moderate levels of Sox9 expression with some cells exhibiting higher expression (Figure 8d,d′). Thus, GFAP efficiently labeled astrocytes in the marmoset cerebellar cortex while S100β, GS, and Sox9 were also present, but showed variable intensity across cerebellar cortex layers and astrocyte types.

Variation in gene expression in the marmoset cerebellar cortex

To better understand the differential expression of astrocytic proteins in BGs and VAs, we characterized the localization of additional proteins known to be expressed by rodent cerebellar astrocytes (Farmer et al., 2016). The differential expression of astrocytic proteins in these cells could be easily identified because of the anatomical separation of BGs and VAs in the cerebellar cortex. As in rodents, BGs showed higher levels of the AMPA receptor GluA1 and Kir4.1, corresponding well to the position of calbindin-positive Purkinje cell soma and dendrites in the ML (Figure 9A,B) (Farmer et al., 2016). VAs, but not BGs, were also enriched in EAAT2 and AQP4 (Figure 9A,B). Thus, the pattern of expression of astrocytic proteins in the marmoset cerebellar cortex closely matched those of the rodent cerebellar cortex.

3.1.4 | Interactions of astrocytes with cerebrovasculature, neurons, and microglia

Astrocytes have complex interactions with cells and structures within their surrounding microenvironment. To begin to understand these interactions, we imaged astrocytes and other structures and cell types. Based on our findings that showed astrocytic processes projecting to blood vessels, we followed up on marmoset endfoot structures. The endfoot is a specialized astrocytic structure that surrounds endothelial cells, pericytes, and smooth muscle cells (in larger diameter vessels) (Figure 10A) and contributes to the blood–brain barrier (Simard & Nedergaard, 2004). Like in the rodent and human, the marmoset endfoot is highly enriched in GFAP expression (Figure 10B) (Oberheim et al., 2009). GFAP-labeled endfeet showed a rosette morphology (diameter between 5 and 10 μm) and each astrocyte often generated more than one rosette (Figures 2D and 10B). In contrast to GFAP, we found variable expression of S100β at the endfoot. Whereas some endfeet showed high S100β intensity, others had low expression (Figure 10b yellow and red circle, respectively). Endfeet can be identified by a polarized and increased expression of AQP4 and Kir4.1 (Nagelhus et al., 2004; Nielsen et al., 1997; Yang et al., 2011). Higher magnification imaging of the GFAP-labeled endfeet showed AQP4 is juxtaposed to perivascular laminin expression in the basement membrane (Figure 10C). As with AQP4, Kir4.1 was also enriched in the endfoot compartment (Figure 10D).

In addition to the close interactions between astrocytes and blood vessels, we also observed close interdigitation of astrocytic processes with neurons (Figure 10E–I) and those of microglia throughout cortex, hippocampus, and cerebellum (Figure 10J–L). This was revealed through labeling for the calcium-binding protein Iba1 found in microglia and microtubule-associated protein 2 (MAP2), the potassium channel Kv2.1, and calcium-binding protein Calbindin found in neurons. Subpial astrocytes intermingled with dendrites in layer I of the cerebral cortex and cell bodies of cortical neurons in layer II labeled with MAP2 (Figure 10E,e′, white arrowheads). The neuronal membrane channel and marker Kv2.1 was particularly effective in highlighting the complex relationship of astrocytes with neuronal soma and proximal dendrites (Figure 10F,f′). In the hippocampus, astrocytic processes penetrated the dense network of dendrites and pyramidal cell bodies in the S. pyramidale (Figure 10G,g′). The selective enrichment of Kv2.1 in some neurons in the S. radiatum also allowed close cellular interactions to be

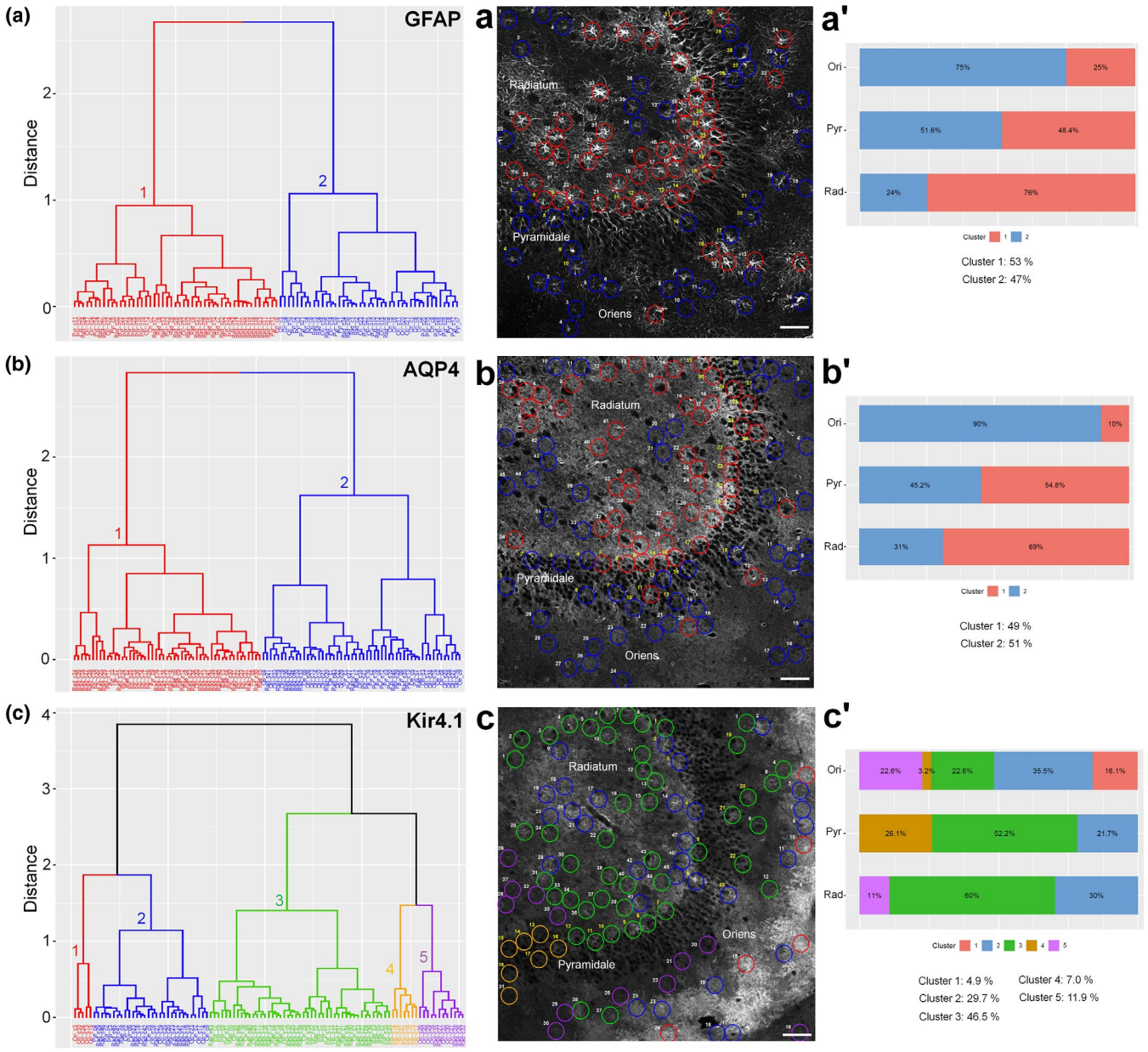

FIGURE 7 Heterogeneity of hippocampal astrocytes. Hierarchical clustering algorithm identified different astrocytic clusters based on the KS distance displayed in the dendrogram (left panel on each row) for GFAP (A), AQP4 (B), and Kir4.1 (C). The spatial organization of astrocytes within clusters is represented at the right side of each image (a–c). Scale bars: 50 μm. Each astrocyte was detected using GS expression and it was assigned in S. radiatum, S. pyramidale, and S. oriens. Each astrocyte was identified with a number, S. radiatum and S. oriens in white and S. pyramidale in yellow. Analysis of GS, EAAT2, and GAT3 can be found in Figure S6. Every astrocyte within a cluster was identified and assigned a number with a particular color. The percentage of cells in each cluster in the S. oriens (Ori), S. pyramidale (Pyr), and S. radiatum (Rad) is shown in a′–c′

observed (Figure 10H,h′). In the cerebellum, the complex dendritic arbor of Purkinje neurons visualized by calbindin labeling was closely associated with radial fibers of BG (Figure 10I). Some BG and VA processes projected alongside Purkinje dendrites and axons, respectively (Figure 10I,i′, white arrowheads).

As astrocytes and microglia are known to have important cellular interactions in the CNS (Bouvier & Murai, 2015), we co-labeled for microglia and astrocytes. We found astrocytes have close relationships with both blood vessel-associated microglia (VAM) and other parenchymal microglia. VAM are parenchymal microglia juxtaposed to cerebral blood vessels just outside of the basal lamina (Graeber & Streit, 1990; Koizumi et al., 2019). Some VAM were observed surrounding blood vessels and interacting with astrocytes (Figure 10J,j′, orange arrowheads) while others had cell bodies in direct contact to the blood vessel and endfoot (Figure 10j′,j″, white arrowheads). Parenchymal microglia were uniformly distributed in cerebral cortex (Figure 10k, k') and displayed fine, ramified processes with a domain diameter of ~70 μm. In the hippocampus,

parenchymal microglia showed smaller domains than in cortex (~40–55 μm). Parenchymal microglia in the cerebral cortex and hippocampus showed close association with astrocytes labeled for GFAP (Figure 10,k′,l′, white arrowheads). Thus, as in other species, marmoset astrocytes showed intricate interactions with microglia, likely reflecting their close functional interaction in the healthy and diseased brain.

4 | DISCUSSION

In this study we investigated the organization, structure, and molecular diversity of astrocytes in the adult marmoset brain. We were pleased to find that many common astrocyte labels used in rodent studies were useful for studying astrocytes in the marmoset cerebral cortex, hippocampus, and cerebellum. Marmoset

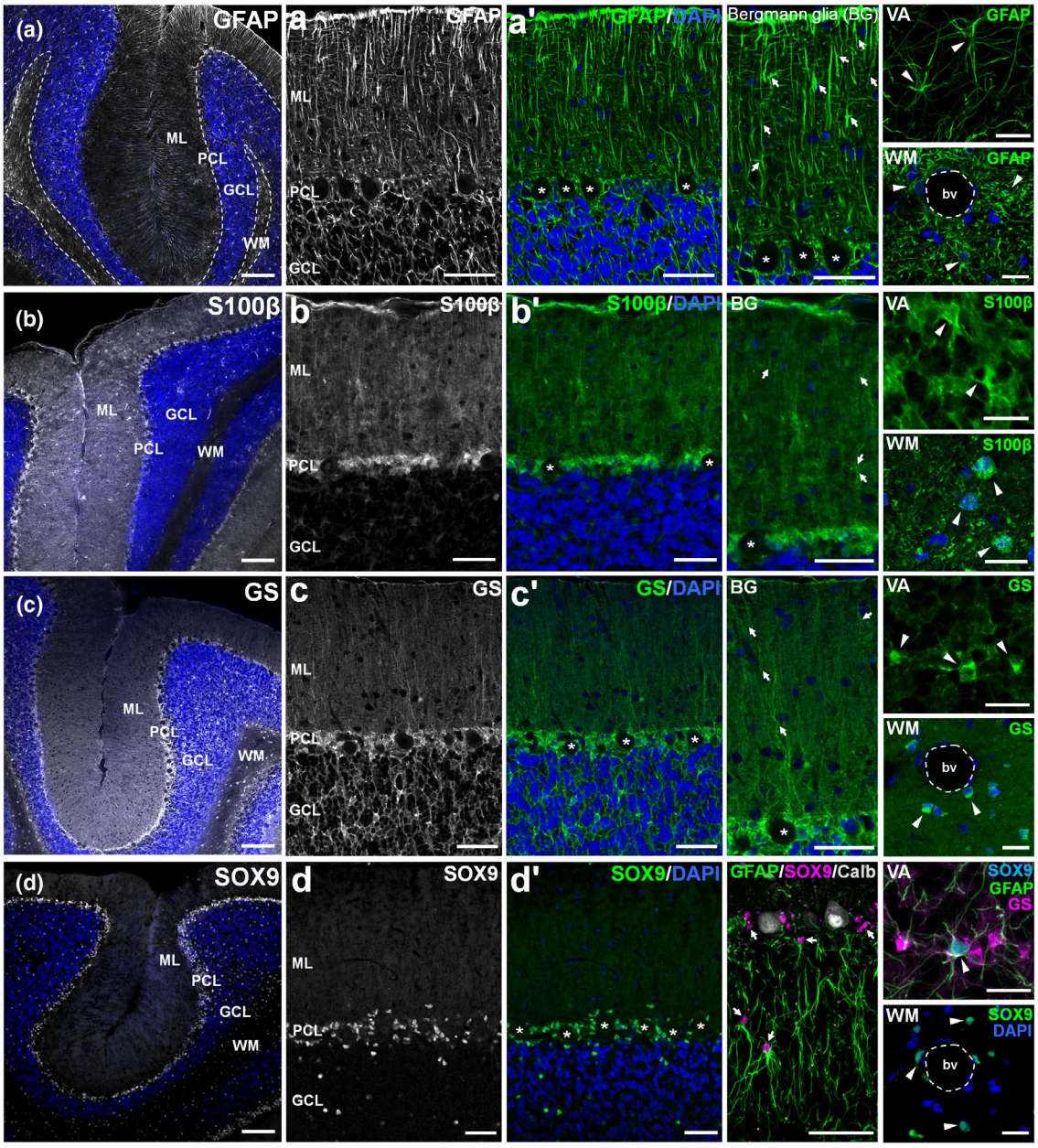

FIGURE 8 Expression of astrocytic markers in the marmoset cerebellum. Labeling of coronal sections of the marmoset cerebellar cortex and white matter with antibodies against GFAP (A), S100β (B), GS (C), and Sox9 (D). General images show the molecular layer (ML), Purkinje cell layer (PCL), granule cell layer (GCL), and white matter (WM). Each immunolabel is contrasted with DAPI staining of nuclei (blue). Scale bars: 100 μm. Panels (a–d) show higher magnification images while panels (a′–d′) show labels with respect to DAPI signal (third panel). Purkinje cell bodies are indicated with white asterisks. Scale bars: 50 μm. Magnifications of individual Bergmann glia cells (BG), velate astrocytes (VA), and astrocytes located within the white matter (WM) are shown in the last panel and they are indicated with white arrows (BG) and arrowheads. Note the presence of many lateral processes of Bergmann glia (white arrows in GFAP, S100β, and GS staining). Calbindin (Calb, gray staining) was used as a Purkinje cell marker. Scale bars: 50 μm in Bergmann glia and 20 μm in VA and WM images. bv, blood vessel

astrocytes showed complex organization and clear inter-regional and intra-regional variation in expression of astrocytic labels. This molecular variation in marmoset astrocytes was accompanied by some unique structural differences among these cells and complex interactions with blood vessels, neurons, and microglia. This study increases our understanding of marmoset astrocytes and helps to understand the complex properties of astrocytes in the primate CNS. It should be noted that robust specific controls for the antibodies used in this study are not available. Also, while the antibodies have been extensively used in rodents, they have not been previously validated in marmoset tissues. However, the similarities in labeling of certain astrocytic populations and specific astrocytic compartments (i.e., nucleus, cytoplasm, soma, fine processes, and endfeet) between rodent and marmoset astrocytes and conservation of the antigens/proteins used to generate the antibodies, provide confidence that the signals detected are specific to the intended antigen. Indeed, amino acid sequence alignment of rodent and marmoset astrocytic proteins shows that sequences recognized by antibodies used in this study had at least 80% conservation. Where residues were not conserved, they were replaced by conservative amino acids that have similar biochemical properties. Ultimately, future validation experiments, for example using gene-knock-out approaches, will be useful in confirming the specificity of the antibodies in marmosets.

Emerging evidence shows that astrocytes comprise a heterogeneous group of cells in the mammalian CNS. Astrocytes in different regions of the brain have substantial variation in gene expression and physiology that is attributable, in part, to their developmental origin (Hochstim et al., 2008; Oberheim et al., 2012; Zhang & Barres, 2010). Multiple astrocyte subtypes have been described across the rodent CNS including protoplasmic, fibrous, and velate astrocytes and polarized astrocytes including BG and Müller glia that likely contribute to brain region-specific physiology (Emsley

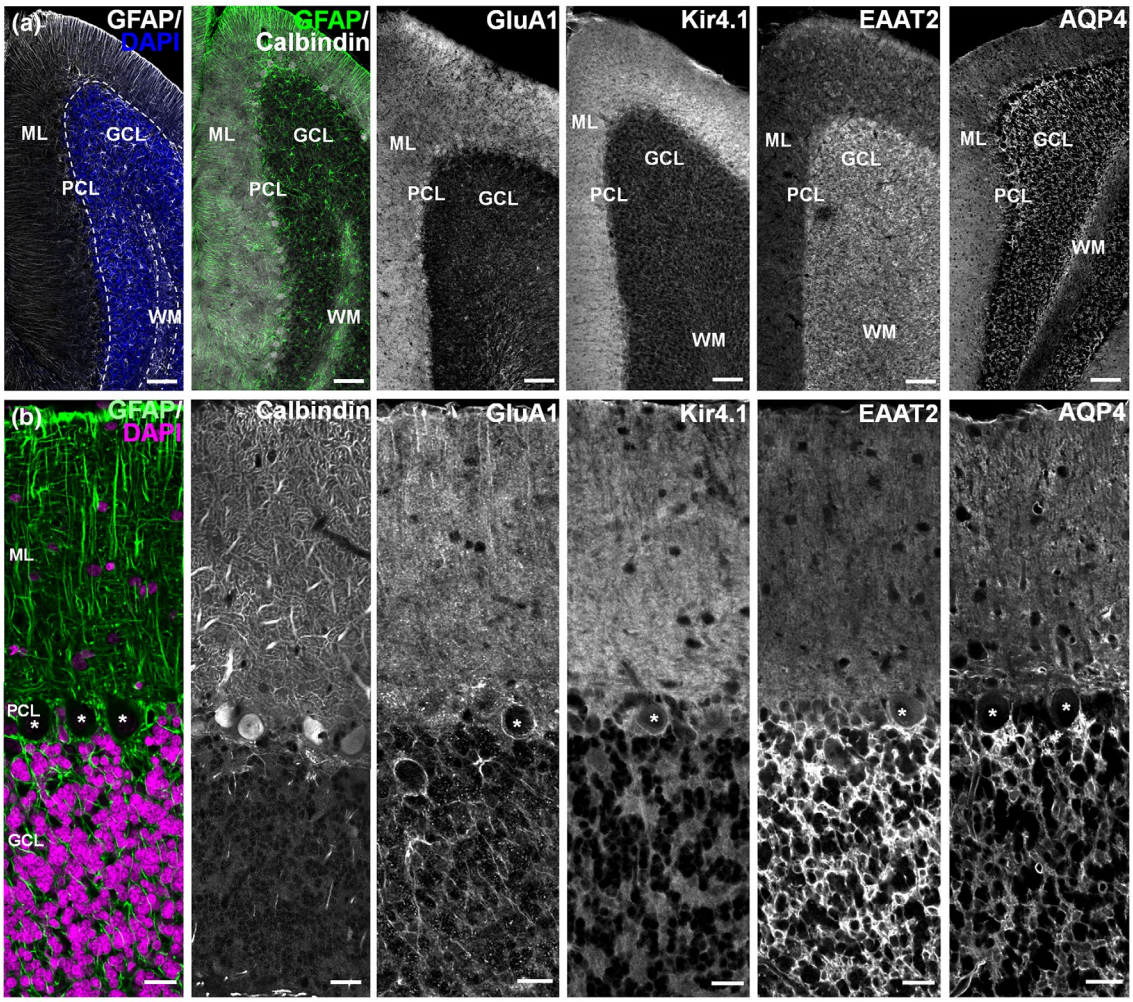

FIGURE 9 Molecular heterogeneity of astrocytes in the marmoset cerebellum. (A) Lower magnification images showing labeling for astrocytic proteins with respect to the molecular layer (ML), Purkinje cell layer (PCL), granule cell layer (GCL), and white matter (WM). Calbindin is used as a Purkinje cell marker. DAPI staining (blue) shows the nuclear staining of interneurons in the ML and granule cells in GCL. Scale bar: 100 μm. (B) Detailed images of ML and GCL stained with specific markers for Bergmann glia (BG) such as GluA1, Kirk4.1, and velate astrocytes (VA) such as AQP4. EAAT2 was expressed in both BGs and VAs with higher expression in VAs. Purkinje cell bodies are indicated with a white asterisk. Scale bar: 20 μm. bv, blood vessel

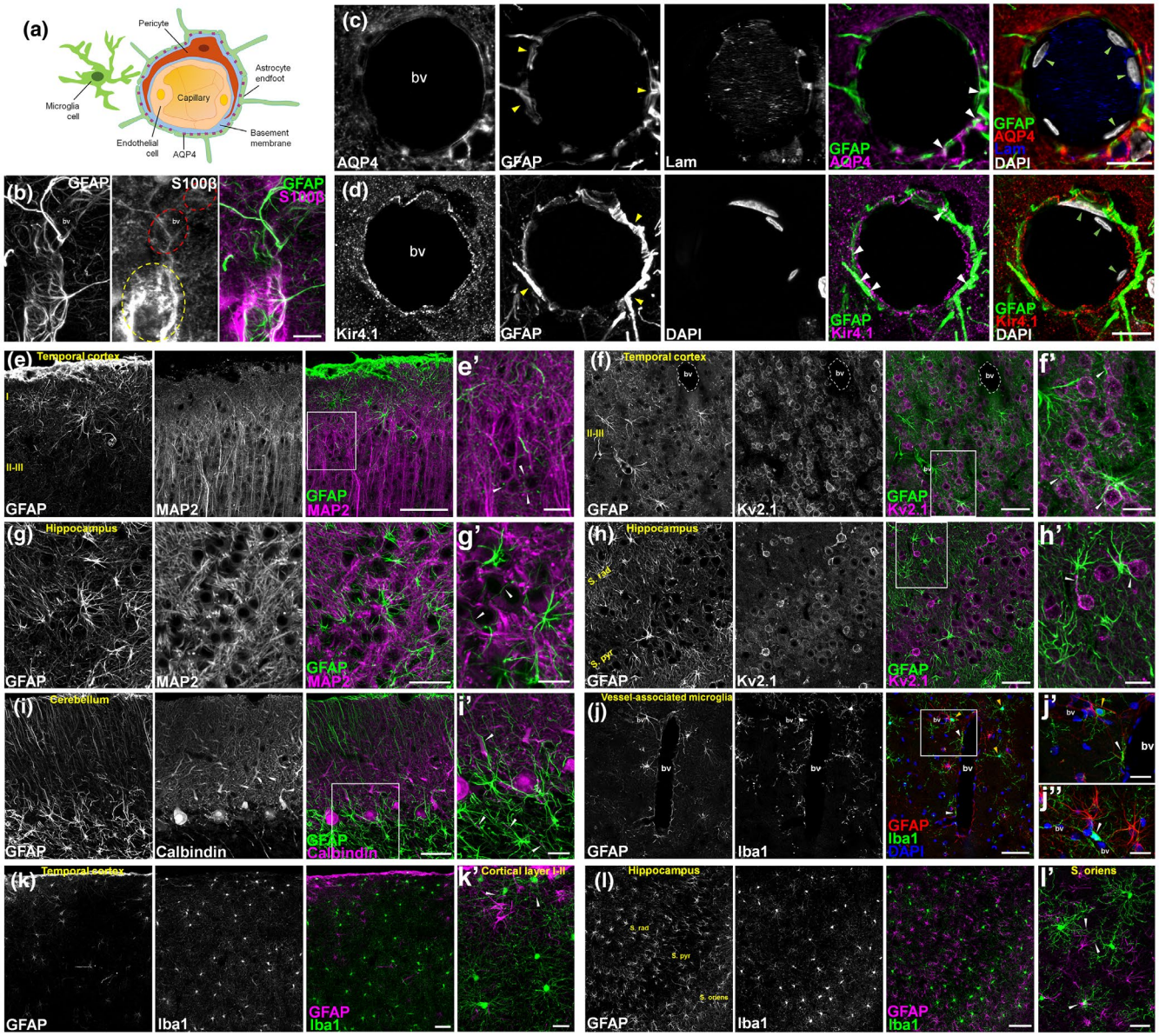

FIGURE 10 Interactions of marmoset astrocytes with capillaries, neurons, and microglia. (A) Schema showing the gliovascular unit and blood vessel-associated microglia. (B) GFAP and S100β labeling in astrocytic processes and endfeet surrounding a capillary in the marmoset cortex. Yellow circle shows high S100β expression and red circles highlight low S100β expression. Scale bar: 20 μm. (C) Cross-sectional view of a capillary in the marmoset hippocampus displaying expression of AQP4 and GFAP at the astrocyte endfeet. Yellow arrowheads indicate GFAP expression at endfeet and white arrowheads indicate areas of co-localization between GFAP and AQP4. Laminin (Lam) and DAPI labels show the basement membrane and nuclei of endothelial cells and pericytes (green arrowheads), respectively. Scale bars: 5 μm. (D) Cross-sectional view of a capillary showing expression of Kir4.1 and GFAP at astrocyte endfeet and DAPI in endothelial cell and pericyte nuclei. Yellow arrowheads indicate GFAP expression, white arrowheads show areas of co-localization between GFAP and Kir4.1, and green arrowheads highlight nuclei. Scale bars: 5 μm. (E–I) Co-labeling of GFAP with neuronal markers including MAP2 (E, temporal cortex; G, hippocampus), Kv2.1 (F, temporal cortex; H hippocampus), and Calbindin (I, cerebellum). Higher magnification images are shown to the right of each panel (panels e′–i′). White arrowheads highlight the tight spatial neuronal-astrocyte interaction. (J–L) Co-labeling of GFAP with the microglial marker Iba1 in temporal cortex (J and K) and hippocampus (L). Images to the right of each panel (panels j′–l′) show higher magnifications. (J) Vessel-associated microglia. Higher magnification images show microglia around the blood vessel (orange arrowheads) and microglia attached at the capillary (white arrowheads) (panels j′, j″). White arrowheads highlight the close spatial microglial–astrocyte interaction. Scale bars in panels E–L are 50 μm and e′–l′ are 20 μm. bv, blood vessel

& Macklis, 2006). Recent investigations in rodents have shown significant intra-regional variation in gene expression in astrocytes (Batiuk et al., 2020; Bayraktar et al., 2020). This unforeseen astrocyte diversity is believed to create specialized astrocyte microenvironments near specific neuronal subtypes and circuitry (Farmer & Murai, 2017). However, the conservation of this astrocyte diversity across species, and importantly, in primates remains to be better understood.

Historically, protoplasmic astrocytes in the cerebral cortex have been thought to constitute a uniform cell population important for brain structural integrity and homeostasis. However, recent investigations have revealed that astrocytes in cortical layers have distinct morphologies with differences in territorial volume, cell orientation, arborization, and differences in gene expression (Lanjakornsiripan et al., 2018). This may be due to the layer-specific features of neurons within cerebral cortex that have specific afferent, efferent, and local connectivity. Astrocytes located in layers II/III have a greater territorial volume and form larger "glio-neuronal" units than astrocytes in cortical layer VI (Clavreul et al., 2019; Lanjakornsiripan et al., 2018). Furthermore, perisynaptic astrocytic processes have greater synaptic ensheathment in layer II/III than layer VI (Lanjakornsiripan et al., 2018). This is consistent with differences in transcriptional profiles of astrocytes in these cortical layers (John Lin et al., 2017; Morel et al., 2019). Astrocytes may interact differently with neighboring synapses depending on layer-specific molecular and structural information. This may enable differential modulation of synaptic function and plasticity for example through regulation of neurotransmitter clearance, ion homeostasis, or release of neuroactive molecules. Interesting, a recent study showed that a common progenitor clone can produce protoplasmic and pial astrocytes, arguing against specific intrinsic genetic programs that create different astrocyte types that reside in disparate locations (Clavreul et al., 2019). This suggests that some astrocytes adapt to local environmental cues to optimize their molecular configuration (Clavreul et al., 2019; Farmer et al., 2016) and is consistent with Lanjakornsiripan et al. (2018) showing that neuronal layering is a prerequisite for the establishment of the layer-specific properties of cortical astrocytes. The patchy expression of astrocyte proteins such as Kir4.1 and EAAT2 observed in this study can reasonably be explained by this (Figure 3). EAAT2 and EAAT1 are known to be differentially expressed during CNS development and maturation in the rodent brain (Furuta et al., 1997; Lehre et al., 1995; Rothstein et al., 1994). EAAT1 has been found to be highly expressed in middle cortical layers at postnatal day 1 and its concentrated distribution was shown to dissipate by postnatal day 24. EAAT2, in contrast, has prominent expression in periventricular and deep cortical layers at postnatal day 1 but more uniform expression by postnatal day 24 (Regan et al., 2007). EAAT2 showed patchy expression in cortical layers in the adult marmoset and had especially low expression in layer I (Figure 3A), as previously has been reported by Rothstein et al. (1994). Kir4.1 also showed variable expression and its distribution resembled what has been reported for Kir4.1 in the rat where it is more enriched in certain cortical layers (Moroni et al., 2015). From our cluster analysis, astrocytes expressing similar levels of molecules such as EAAT2 and Kir4.1 show an especially interesting pattern of organization. In the future, it will be interesting to study whether these astrocytes have shared developmental origins or have common signaling mechanisms that actively control their molecular profile.

Our analysis also showed that marmosets contain both pial and subpial ILAs in the cerebral cortex. Interlaminar astrocytes in human cortex were first described by Andriezen using Golgi staining (Andriezen, 1893). However, these astrocytes received little attention for nearly a century until Colombo et al. analyzed samples from New World monkeys (*platyrrhini)* and showed that ILA processes were GFAP immunoreactive (Colombo et al., 1995). Recently, Falcone et al., performed a comprehensive study of pial and subpial astrocytes from 46 mammalian species, including 22 primates (*platyrrhini* and Old World (*catarrhine*) monkeys) but not the common marmoset (*C. jacchus*). We found that the complexity of astrocytes residing in the pia mater of the cerebral cortex of the common marmoset was similar to descriptions made by Falcone et al. (2019) with respect to other monkey species belonging to Family Callitrichidae (*Cebuella pigmaea* and *Saginus imperator*) in terms of cell position, and number and length of processes. However, marmoset ILAs appear to be shorter than those observed in the larger monkey species *Cebus apella* and *Saimiri sciureus* (Colombo et al., 1995). Thus, the marmoset cortex contains ILAs with similar features to those in other non-human primate species and humans, opening the possibility of conserved function related to their structural features. Taking advantage of the superficial positioning of ILAs in the lissencephalic marmoset brain, *in vivo* calcium imaging experiments are likely to provide important insight into the physiological dynamics of this interesting cell population.

In the hippocampus, we found that astrocytes showed different morphologies depending on their location within area CA1. In general, marmoset protoplasmic astrocytes in the S. radiatum showed a stellate morphology with processes leaving round-shaped cell bodies (Figure 5J). This is similar to what has been reported for rodent astrocytes in the S. radiatum of CA1 that show exclusive domain/territory organization (Bushong et al., 2002; Nixdorf-Bergweiler et al., 1994). Interestingly, astrocytes located at the interface of the S. radiatum and S. pyramidale displayed a unique structure, containing long, highly polarized processes interlacing between pyramidal cell somas and with sparse side branches (Figure 5I,L,M). This unique structural adaptation may enable astrocytes to directionally propagate information across the pyramidal cell layer and between the S. radiatum and S. oriens. As was found with in the cerebral cortex, protoplasmic astrocytes showed variable expression of some known astrocyte proteins. Of particular interest was the discovery of an enriched band of labeling of molecules such as EAAT2, Kir4.1, GFAP, and AQP4, at the boundary of the S. radiatum/S. pyramidale (Figures 5, 6 and S6). It is possible that astrocytic processes in this specific region may have specialized properties in maintaining glutamate, potassium, and intra/extracellular water levels. The high expression of EAAT2 in the S. oriens and S. radiatum has been previously reported in rodent brain (Lehre et al., 1995; Rothstein et al., 1994). The relatively high expression of AQP4 may contribute to neurotransmitter and ion homeostasis which are known to impact synaptic function and long-term plasticity (Scharfman & Binder, 2013). Interestingly, AQP4 KO mice have been shown to have a selective impairment in BDNF-dependent LTP and LTD at Schaffer collateral synapses onto CA1 pyramidal cells (Skucas et al., 2011) and have cognitive deficits in object recognition memory but not contextual fear or spatial

memory (Skucas et al., 2011). AQP4 KO mice have increased extracellular space (ECS) which can affect synaptic transmission (Binder et al., 2004) potentially through inability of astrocytes to uptake glutamate (Zeng et al., 2007). This is consistent with findings that ECS and cell volume changes occur in response to altered extracellular osmolarity and are associated with seizure activity (Binder et al., 2004). The high expression of Kir4.1 in S. oriens has been previously reported in the rodent brain (Takumi et al., 1995). Polarized Kir4.1 expression may also support greater uptake and redistribution of potassium during times of high neuronal activity (Binder et al., 2006; Djukic et al., 2007). Further experimentation is needed to understand the physiological implications for the enrichment of molecules such as AQP4, Kir4.1, and glutamate transporters, in this specific region.

BG in the ML and VA in the GCL are two main types of astrocytes in the cerebellar cortex. During development, BG play a crucial role in nearly all phases of cerebellar corticogenesis such as foliation, orientation, stratification of granule cells, neuronal migration, neurite outgrowth, and synaptogenesis (Buffo & Rossi, 2013). In adulthood, BG are important for maintaining synaptic stability (Iino et al., 2001; Saab et al., 2012), extracellular ion homeostasis (Wang et al., 2012), metabolic function, and plasticity, and are needed for neuroprotection of Purkinje cells (Poblete-Naredo et al., 2011). Marmoset BG show high expression of the AMPA receptor GluA1 and the potassium channel Kir4.1 (Figure 9A,B). This result is consistent with previous reports in rats and mice (Matsui et al., 2005; Saab et al., 2012; Takumi et al., 1995). Similar to the rodent, we found dichotomous expression of several proteins in BG and VAs, with enriched expression of GluA1, Kir4.1 in BGs, and AQP4 in VAs (Farmer et al., 2016). EAAT2 was found in BGs and VAs with higher expression in VAs. Previous reports have shown that EAAT2 was enriched in BG more than VAs in rat brain (Lehre et al., 1995; Rothstein et al., 1994). This suggests some differential distribution across species. Immunoreactivity for GS (Figure 8C, BG) and glutamate receptors/transporters GluA1 and EAAT2 (Figure 9A,B) in BG processes in the ML and near Purkinje cell body suggests that marmoset BGs, like in other species, are geared toward glutamate detection, recovery, and signaling related to parallel and climbing fiber glutamatergic transmission (Maragakis & Rothstein, 2004). BG fibers of early postnatal rodents are smooth and lack lateral processes (Grosche et al., 2002), however, lateral appendages appear after the first week of life potentially associated with an increase in neuronal activity in the cerebellum (Bender et al., 2020; Grosche et al., 1999, 2002). Recently, lateral appendages have been involved in a new type of plasticity mediated by GluA1 AMPARs and induced by emotional stress (Bender et al., 2020). Thus, lateral appendages of BG could be a new target to investigate cerebellar plasticity and learning. Compared with its rodent counterpart, the adult marmoset ML has a strikingly complex network of long lateral appendages emerging from main radial BG processes, visualized by GFAP and to a lesser extent GS, and S100β staining (Figure 9). Further experimentation using fluorescent dye filling, or viral/transgene-mediated expression of genetically encoded reporters would be necessary for detailed investigation of lateral processes and to make structural comparisons with processes observed in the rodent (Grosche et al., 1999, 2002). We also detected complex relationships of marmoset astrocytes with cerebrovasculature, neurons, and microglia. Several neuronal and microglia markers (i.e., MAP2, Kv2.1, and Calbindin in neurons and Iba1 in microglia) were efficient in revealing their intricate relationship with astrocytes within the brain parenchyma. Astrocytes also showed intricate GFAP-labeled endfoot structures on capillaries with concentrated Kir4.1, AQP4, and S100β protein. In the human brain, the endfoot more completely encompasses blood vessel, creating a cobblestone pattern along the vasculature (Oberheim et al., 2009). Marmoset endfeet formed rosettes similar to those observed in the rodent brain. Thus, the marmoset endfoot has certain features that more closely resemble structures in the rodent rather than in humans. However, additional investigation is needed to dissect the marmoset endfoot compartment. As in rodents, marmoset protoplasmic astrocytes appeared to respect territorial boundaries with neighboring astrocytes (Figure 3) but were fully interlaced among cell bodies and processes of neurons and microglia (Figure 10). Thus, the mechanisms leading to the organization and spacing of astrocytes may be well preserved among rodents and marmosets. Future investigations involving single-cell RNA-seq (Luecken & Theis, 2019) and multi-label *in situ* hybridization (Lukumbuzya et al., 2019) techniques will enhance our understanding of the molecular profile of marmoset astrocytes and strengthen the basis for experiments that reveal the complex functional properties of this diverse cell population in the CNS.

DECLARATION OF TRANSPARENCY

The authors, reviewers and editors affirm that in accordance to the policies set by the *Journal of Neuroscience Research*, this manuscript presents an accurate and transparent account of the study being reported and that all critical details describing the methods and results are present.

ACKNOWLEDGMENTS

This work was supported by the Canadian Institutes of Health Research (PJT148569, 156247 to K.K.M.); Natural Sciences and Engineering Research Council of Canada (408044-2011 and 69404 to K.K.M.), and a Joint Canada-Israel Research Program Award provided by the International Development Research Centre (IDRC)/ Israel Science Foundation/Canadian Institutes of Health Research/ Azrieli Foundation. G.Q. was supported by a postdoctoral fellowship from the Fonds de recherche du Québec- Santé (FRQS). F.C.P was supported by the National Agency for Research and Development of Chile, through Grant ANID/FONDECYT/POSTDOCTORADO/ No. 3210453 and supported by the AC3E Research Group, UTFSM, through Grant FB-0008.

CONFLICT OF INTEREST

The authors state that they have no conflict of interest to declare.

AUTHOR CONTRIBUTIONS

Y.M. and K.K.M. conceptualized the project, formally analyzed the data, and wrote original drafts and revised versions of the published work. F.C.P. developed software and resources for performing statistical analysis of astrocyte heterogeneity by Y.M. G.Q. contributed to methodology and tissue resources for the study.

PEER REVIEW

The peer review history for this article is available at https://publons.com/publon/10.1002/jnr.24967.

DATA AVAILABILITY STATEMENT

The data that support the findings of this study are available from the corresponding author, KM, upon reasonable request.

REFERENCES

Andriezen, W. L. (1893). The neuroglia elements in the human brain. *British Medical Journal*, *2*(1700), 227–230. https://doi.org/10.1136/bmj.2.1700.227

Aron Badin, R. (2018). Nonhuman primate models of Huntington's disease and their application in translational research. *Methods in Molecular Biology*, *1780*, 267–284. https://link.springer.com/protocol/10.1007%2F978-1-4939-7825-0_14

Batiuk, M. Y., Martirosyan, A., Wahis, J., de Vin, F., Marneffe, C., Kusserow, C., Koeppen, J., Viana, J. F., Oliveira, J. F., Voet, T., Ponting, C. P., Belgard, T. G., & Holt, M. G. (2020). Identification of region-specific astrocyte subtypes at single cell resolution. *Nature Communications*, *11*, 1220. https://www.nature.com/articles/s41467-019-14198-8

Bayraktar, O. A., Bartels, T., Holmqvist, S., Kleshchevnikov, V., Martirosyan, A., Polioudakis, D., Ben Haim, L., Young, A. M. H., Batiuk, M. Y., Prakash, K., Brown, A., Roberts, K., Paredes, M. F., Kawaguchi, R., Stockley, J. H., Sabeur, K., Chang, S. M., Huang, E., Hutchinson, P., … Rowitch, D. H. (2020). Astrocyte layers in the mammalian cerebral cortex revealed by a single-cell in situ transcriptomic map. *Nature Neuroscience*, *23*(4), 500–509. https://doi.org/10.1038/s41593-020-0602-1

Ben Haim, L., & Rowitch, D. H. (2017). Functional diversity of astrocytes in neural circuit regulation. *Nature Reviews Neuroscience*, *18*(1), 31–41. https://www.nature.com/articles/nrn.2016.159

Bender, C. L., Sun, X., Farooq, M., Yang, Q., Davison, C., Maroteaux, M., Huang, Y.-S., Ishikawa, Y., & Liu, S. J. (2020). Emotional stress induces structural plasticity in Bergmann glial cells via an AC5-CPEB3-GluA1 pathway. *Journal of Neuroscience*, *40*(17), 3374–3384. https://www.jneurosci.org/content/40/17/3374.long

Binder, D. K., Oshio, K., Ma, T., Verkman, A. S., & Manley, G. T. (2004). Increased seizure threshold in mice lacking aquaporin-4 water channels. *NeuroReport*, *15*(2), 259–262. https://doi.org/10.1097/00001756-200402090-00009

Binder, D. K., Papadopoulos, M. C., Haggie, P. M., & Verkman, A. S. (2004). In vivo measurement of brain extracellular space diffusion by cortical surface photobleaching. *Journal of Neuroscience*, *24*(37), 8049–8056. https://www.jneurosci.org/content/24/37/8049.long

Binder, D. K., Yao, X., Zador, Z., Sick, T. J., Verkman, A. S., & Manley, G. T. (2006). Increased seizure duration and slowed potassium kinetics in mice lacking aquaporin-4 water channels. *Glia*, *53*(6), 631–636. https://doi.org/10.1002/glia.20318

Bouvier, D. S., & Murai, K. K. (2015). Synergistic actions of microglia and astrocytes in the progression of Alzheimer's disease. *Journal of Alzheimer's Disease*, *45*(4), 1001–1014. https://doi.org/10.3233/JAD-143156

Budoff, S. A., Yano, K. M., de Mesquita, F. C., Doerl, J. G., de Santana, M. B., Nascimento, M. S., Kunicki, A. C., & de Araújo, M. F. (2019). Astrocytic response to acutely- and chronically-implanted microelectrode arrays in the marmoset (*Callithrix jacchus*) brain. *Brain Sciences*, *9*(2), 19. https://www.mdpi.com/2076-3425/9/2/19

Buffo, A., & Rossi, F. (2013). Origin, lineage and function of cerebellar glia. *Progress in Neurobiology*, *109*, 42–63. https://doi.org/10.1016/j.pneurobio.2013.08.001

Bushong, E. A., Martone, M. E., Jones, Y. Z., & Ellisman, M. H. (2002). Protoplasmic astrocytes in CA1 stratum radiatum occupy separate anatomical domains. *Journal of Neuroscience*, *22*(1), 183–192. https://www.jneurosci.org/content/22/1/183.long. https://doi.org/10.1523/JNEUROSCI.22-01-00183.2002

Chai, H., Diaz-Castro, B., Shigetomi, E., Monte, E., Octeau, J. C., Yu, X., Cohn, W., Rajendran, P. S., Vondriska, T. M., Whitelegge, J. P., Coppola, G., & Khakh, B. S. (2017). Neural circuit-specialized astrocytes: Transcriptomic, proteomic, morphological, and functional evidence. *Neuron*, *95*(3), 531–549.e9. https://www.cell.com/neuron/fulltext/S0896-6273(17)30553-6?_returnURL=https%3A%2F%2Flinkinghub.elsevier.com%2Fretrieve%2Fpii%2FS0896627317305536%3Fshowall%3Dtrue

Chan-Palay, V., & Palay, S. L. (1974). *Cerebellar cortex -cytology and organization*. Springer-Verlag Berlin Heidelberg. https://doi.org/10.1007/978-3-642-65581-4. https://www.springer.com/gp/book/9783642655838

Chaudhry, F. A., Lehre, K. P., van Lookeren Campagne, M., Ottersen, O. P., Danbolt, N. C., & Storm-Mathisen, J. (1995). Glutamate transporters in glial plasma membranes: Highly differentiated localizations revealed by quantitative ultrastructural immunocytochemistry. *Neuron*, *15*(3), 711–720. https://doi.org/10.1016/0896-6273(95)90158-2

Clavreul, S., Abdeladim, L., Hernández-Garzón, E., Niculescu, D., Durand, J., Ieng, S.-H., Barry, R., Bonvento, G., Beaurepaire, E., Livet, J., & Loulier, K. (2019). Cortical astrocytes develop in a plastic manner at both clonal and cellular levels. *Nature Communications*, *10*(1), 4884. https://www.nature.com/articles/s41467-019-12791-5

Colombo, J. A., Fuchs, E., Hartig, W., Marotte, L. R., & Puissant, V. (2000). "Rodent-like" and "primate-like" types of astroglial architecture in the adult cerebral cortex of mammals: A comparative study. *Anatomy and Embryology (Berl)*, *201*(2), 111–120. https://link.springer.com/article/10.1007%2FPL00008231

Colombo, J. A., Gayol, S., Yanez, A., & Marco, P. (1997). Immunocytochemical and electron microscope observations on astroglial interlaminar processes in the primate neocortex. *Journal of Neuroscience Research*, *48*(4), 352–357. https://doi.org/10.1002/(SICI)1097-4547(19970515)48:4<352:AID-JNR7>3.0.CO;2-A. https://onlinelibrary.wiley.com/doi/abs/https://doi.org/10.1002/%28SICI%291097-4547%2819970515%2948%3A4%3C352%3A%3AAID-JNR7%3E3.0.CO%3B2-A?sid=nlm%3Apubmed

Colombo, J. A., Yanez, A., Puissant, V., & Lipina, S. (1995). Long, interlaminar astroglial cell processes in the cortex of adult monkeys. *Journal of Neuroscience Research*, *40*(4), 551–556. https://doi.org/10.1002/jnr.490400414

Corkrum, M., Rothwell, P. E., Thomas, M. J., Kofuji, P., & Araque, A. (2019). Opioid-mediated astrocyte-neuron signaling in the nucleus accumbens. *Cells*, *8*(6), 586. https://www.mdpi.com/2073-4409/8/6/586

de la Mothe, L. A., Blumell, S., Kajikawa, Y., & Hackett, T. A. (2006). Cortical connections of the auditory cortex in marmoset monkeys: Core and medial belt regions. *Journal of Comparative Neurology*, *496*(1), 27–71. https://doi.org/10.1002/cne.20923

Derouiche, A., & Frotscher, M. (1991). Astroglial processes around identified glutamatergic synapses contain glutamine synthetase: Evidence for transmitter degradation. *Brain Research*, *552*(2), 346–350. https://doi.org/10.1016/0006-8993(91)90103-3

Djukic, B., Casper, K. B., Philpot, B. D., Chin, L. S., & McCarthy, K. D. (2007). Conditional knock-out of Kir4.1 leads to glial membrane depolarization,

inhibition of potassium and glutamate uptake, and enhanced short-term synaptic potentiation. *Journal of Neuroscience*, *27*(42), 11354–11365. https://doi.org/10.1523/JNEUROSCI.0723-07.2007

Emsley, J. G., & Macklis, J. D. (2006). Astroglial heterogeneity closely reflects the neuronal-defined anatomy of the adult murine CNS. *Neuron Glia Biology*, *2*(3), 175–186. https://www.ncbi.nlm.nih.gov/pmc/articles/PMC1820889/pdf/nihms12906.pdf

Falcone, C., Wolf-Ochoa, M., Amina, S., Hong, T., Vakilzadeh, G., Hopkins, W. D., Hof, P. R., Sherwood, C. C., Manger, P. R., Noctor, S. C., & Martínez-Cerdeño, V. (2019). Cortical interlaminar astrocytes across the therian mammal radiation. *Journal of Comparative Neurology*, *527*(10), 1654–1674. https://doi.org/10.1002/cne.24605

Farmer, W. T., Abrahamsson, T., Chierzi, S., Lui, C., Zaelzer, C., Jones, E. V., Bally, B. P., Chen, G. G., Theroux, J.-F., Peng, J., Bourque, C. W., Charron, F., Ernst, C., Sjostrom, P. J., & Murai, K. K. (2016). Neurons diversify astrocytes in the adult brain through sonic hedgehog signaling. *Science*, *351*(6275), 849–854. https://doi.org/10.1126/science.aab3103

Farmer, W. T., & Murai, K. (2017). Resolving astrocyte heterogeneity in the CNS. *Frontiers in Cellular Neuroscience*, *11*, 300. https://doi.org/10.3389/fncel.2017.00300

Furuta, A., Rothstein, J. D., & Martin, L. J. (1997). Glutamate transporter protein subtypes are expressed differentially during rat CNS development. *Journal of Neuroscience*, *17*(21), 8363–8375. https://doi.org/10.1523/jneurosci.17-21-08363.1997

Goldshmit, Y., & Bourne, J. (2010). Upregulation of EphA4 on astrocytes potentially mediates astrocytic gliosis after cortical lesion in the marmoset monkey. *Journal of Neurotrauma*, *27*(7), 1321–1332. https://doi.org/10.1089/neu.2010.1294

Goldshmit, Y., Homman-Ludiye, J., & Bourne, J. A. (2014). EphA4 is associated with multiple cell types in the marmoset primary visual cortex throughout the lifespan. *European Journal of Neuroscience*, *39*(9), 1419–1428. https://doi.org/10.1111/ejn.12514

Graeber, M. B., & Streit, W. J. (1990). Microglia: Immune network in the CNS. *Brain Pathology*, *1*(1), 2–5. https://onlinelibrary.wiley.com/doi/abs/10.1111/j.1750-3639.1990.tb00630.x?sid=nlm%3Apubmed

Grosche, J., Kettenmann, H., & Reichenbach, A. (2002). Bergmann glial cells form distinct morphological structures to interact with cerebellar neurons. *Journal of Neuroscience Research*, *68*(2), 138–149. https://doi.org/10.1002/jnr.10197

Grosche, J., Matyash, V., Moller, T., Verkhratsky, A., Reichenbach, A., & Kettenmann, H. (1999). Microdomains for neuron-glia interaction: Parallel fiber signaling to Bergmann glial cells. *Nature Neuroscience*, *2*(2), 139–143. https://www.nature.com/articles/nn0299_139

Higashi, K., Fujita, A., Inanobe, A., Tanemoto, M., Doi, K., Kubo, T., & Kurachi, Y. (2001). An inwardly rectifying K(+) channel, Kir4.1, expressed in astrocytes surrounds synapses and blood vessels in brain. *American Journal of Physiology-Cell Physiology*, *281*(3), C922–C931. https://journals.physiology.org/doi/full/10.1152/ajpcell.2001.281.3.C922

Hochstim, C., Deneen, B., Lukaszewicz, A., Zhou, Q., & Anderson, D. J. (2008). Identification of positionally distinct astrocyte subtypes whose identities are specified by a homeodomain code. *Cell*, *133*(3), 510–522. https://www.cell.com/cell/fulltext/S0092-8674(08)00396-6?_returnURL=https%3A%2F%2Flinkinghub.elsevier.com%2Fretrieve%2Fpii%2FS0092867408003966%3Fshowall%3Dtrue

Homman-Ludiye, J., & Bourne, J. A. (2017). The marmoset: An emerging model to unravel the evolution and development of the primate neocortex. *Developmental Neurobiology*, *77*(3), 263–272. https://doi.org/10.1002/dneu.22425

Honavar, M., & Lantos, P. L. (1987). Ultrastructural changes in the frontal cortex and hippocampus in the ageing marmoset. *Mechanisms of Ageing and Development*, *41*(1–2), 161–175. https://www.sciencedirect.com/science/article/abs/pii/0047637487900601?via%3Dihub

Iino, M., Goto, K., Kakegawa, W., Okado, H., Sudo, M., Ishiuchi, S., Miwa, A., Takayasu, Y., Saito, I., Tsuzuki, K., & Ozawa, S. (2001). Glia-synapse interaction through Ca2+-permeable AMPA receptors in Bergmann glia. *Science*, *292*(5518), 926–929. https://www.science.org/lookup/doi/10.1126/science.1058827

Jakab, R. L., & Hamori, J. (1988). Quantitative morphology and synaptology of cerebellar glomeruli in the rat. *Anatomy and Embryology (Berl)*, *179*(1), 81–88. https://link.springer.com/article/10.1007%2FBF00305102

John Lin, C.-C., Yu, K., Hatcher, A., Huang, T.-W., Lee, H. K., Carlson, J., Weston, M. C., Chen, F., Zhang, Y., Zhu, W., Mohila, C. A., Ahmed, N., Patel, A. J., Arenkiel, B. R., Noebels, J. L., Creighton, C. J., & Deneen, B. (2017). Identification of diverse astrocyte populations and their malignant analogs. *Nature Neuroscience*, *20*(3), 396–405. https://www.nature.com/articles/nn.4493

Kacerovsky, B. J., & Murai, K. K. (2016). Stargazing: Monitoring subcellular dynamics of brain astrocytes. *Neuroscience*, *323*, 84–95. https://www.sciencedirect.com/science/article/abs/pii/S0306452215006144?via%3Dihub

Kaufman, L., & Rousseeuw, P. J. (2009). *Finding groups in data: An introduction to cluster analysis* (Vol. *344*). Wiley Series in Probability and Statistics. John Wiley & Sons, Inc. https://onlinelibrary.wiley.com/doi/book/10.1002/9780470316801

Khakh, B. S., & Sofroniew, M. V. (2015). Diversity of astrocyte functions and phenotypes in neural circuits. *Nature Neuroscience*, *18*(7), 942–952. https://www.nature.com/articles/nn.4043

Koizumi, T., Kerkhofs, D., Mizuno, T., Steinbusch, H. W. M., & Foulquier, S. (2019). Vessel-associated immune cells in cerebrovascular diseases: From perivascular macrophages to vessel-associated microglia. *Frontiers in Neuroscience*, *13*, 1291. https://doi.org/10.3389/fnins.2019.01291

Lanjakornsiripan, D., Pior, B.-J., Kawaguchi, D., Furutachi, S., Tahara, T., Katsuyama, Y., Suzuki, Y., Fukazawa, Y., & Gotoh, Y. (2018). Layer-specific morphological and molecular differences in neocortical astrocytes and their dependence on neuronal layers. *Nature Communications*, *9*(1), 1623. https://www.nature.com/articles/s41467-018-03940-3

Lehre, K. P., Levy, L. M., Ottersen, O. P., Storm-Mathisen, J., & Danbolt, N. C. (1995). Differential expression of two glial glutamate transporters in the rat brain: Quantitative and immunocytochemical observations. *Journal of Neuroscience*, *15*(3), 1835–1853. http://dx.doi.org/10.1523/jneurosci.15-03-01835.1995

Li, H. W., Zhang, L., & Qin, C. (2019). Current state of research on non-human primate models of Alzheimer's disease. *Animal Models and Experimental Medicine*, *2*(4), 227–238. https://doi.org/10.1002/ame2.12092

Lisman, J., Buzsaki, G., Eichenbaum, H., Nadel, L., Ranganath, C., & Redish, A. D. (2017). Viewpoints: How the hippocampus contributes to memory, navigation and cognition. *Nature Neuroscience*, *20*(11), 1434–1447. https://www.nature.com/articles/nn.4661

Liu, Y., Namba, T., Liu, J., Suzuki, R., Shioda, S., & Seki, T. (2010). Glial fibrillary acidic protein-expressing neural progenitors give rise to immature neurons via early intermediate progenitors expressing both glial fibrillary acidic protein and neuronal markers in the adult hippocampus. *Neuroscience*, *166*(1), 241–251. https://www.sciencedirect.com/science/article/abs/pii/S0306452209020612?via%3Dihub

Luecken, M. D., & Theis, F. J. (2019). Current best practices in single-cell RNA-seq analysis: A tutorial. *Molecular Systems Biology*, *15*(6), e8746. https://www.embopress.org/doi/full/10.15252/msb.20188746

Lukumbuzya, M., Schmid, M., Pjevac, P., & Daims, H. (2019). A Multicolor fluorescence in situ hybridization approach using an extended set of fluorophores to visualize microorganisms. *Frontiers in Microbiology*, *10*, 1383. https://doi.org/10.3389/fmicb.2019.01383

Maragakis, N. J., & Rothstein, J. D. (2004). Glutamate transporters: Animal models to neurologic disease. *Neurobiology of Diseases*,

15(3), 461–473. https://www.sciencedirect.com/science/article/abs/pii/S0969996103002729?via%3Dihub

Martin-Fernandez, M., Jamison, S., Robin, L. M., Zhao, Z., Martin, E. D., Aguilar, J., Benneyworth, M. A., Marsicano, G., & Araque, A. (2017). Synapse-specific astrocyte gating of amygdala-related behavior. *Nature Neuroscience*, *20*(11), 1540–1548. https://doi.org/10.1038/nn.4649

Mashiko, H., Yoshida, A. C., Kikuchi, S. S., Niimi, K., Takahashi, E., Aruga, J., Okano, H., & Shimogori, T. (2012). Comparative anatomy of marmoset and mouse cortex from genomic expression. *Journal of Neuroscience*, *32*(15), 5039–5053. https://doi.org/10.1523/JNEUROSCI.4788-11.2012

Matsui, K., Jahr, C. E., & Rubio, M. E. (2005). High-concentration rapid transients of glutamate mediate neural-glial communication via ectopic release. *Journal of Neuroscience*, *25*(33), 7538–7547. https://www.jneurosci.org/content/25/33/7538.long

Matsuzaki, Y., Konno, A., Mochizuki, R., Shinohara, Y., Nitta, K., Okada, Y., & Hirai, H. (2018). Intravenous administration of the adeno-associated virus-PHP.B capsid fails to upregulate transduction efficiency in the marmoset brain. *Neuroscience Letters*, *665*, 182–188. https://doi.org/10.1016/j.neulet.2017.11.049

Mattison, J. A., & Vaughan, K. L. (2017). An overview of nonhuman primates in aging research. *Experimental Gerontology*, *94*, 41–45. https://doi.org/10.1016/j.exger.2016.12.005

McDermott, K. W., & Lantos, P. L. (1989). The distribution of glial fibrillary acidic protein and vimentin in postnatal marmoset (*Callithrix jacchus*) brain. *Developmental Brain Research*, *45*(2), 169–177. https://doi.org/10.1016/0165-3806(89)90036-9

Minelli, A., DeBiasi, S., Brecha, N. C., Zuccarello, L. V., & Conti, F. (1996). GAT-3, a high-affinity GABA plasma membrane transporter, is localized to astrocytic processes, and it is not confined to the vicinity of GABAergic synapses in the cerebral cortex. *Journal of Neuroscience*, *16*(19), 6255–6264. https://www.jneurosci.org/content/16/19/6255.long. https://doi.org/10.1523/JNEUROSCI.16-19-06255.1996

Missler, M., Eins, S., Bottcher, H., & Wolff, J. R. (1994). Postnatal development of glial fibrillary acidic protein, vimentin and S100 protein in monkey visual cortex: Evidence for a transient reduction of GFAP immunoreactivity. *Developmental Brain Research*, *82*(1–2), 103–117. https://www.sciencedirect.com/science/article/abs/pii/0165380694901538?via%3Dihub

Mitchell, J. F., & Leopold, D. A. (2015). The marmoset monkey as a model for visual neuroscience. *Neuroscience Research*, *93*, 20–46. https://doi.org/10.1016/j.neures.2015.01.008

Miyamoto, S., Abe, R., Endo, Y., & Takeshita, J.-I. (2015). *Ward method of hierarchical clustering for non-Euclidean similarity measures*. Paper presented at the 2015 7th International Conference of Soft Computing and Pattern Recognition (SoCPaR). IEEE. https://ieeexplore.ieee.org/document/7492784

Morel, L., Men, Y., Chiang, M. S. R., Tian, Y., Jin, S., Yelick, J., Higashimori, H., & Yang, Y. (2019). Intracortical astrocyte subpopulations defined by astrocyte reporter Mice in the adult brain. *Glia*, *67*(1), 171–181. https://doi.org/10.1002/glia.23545

Moroni, R. F., Inverardi, F., Regondi, M. C., Pennacchio, P., & Frassoni, C. (2015). Developmental expression of Kir4.1 in astrocytes and oligodendrocytes of rat somatosensory cortex and hippocampus. *International Journal of Developmental Neuroscience*, *47*(Pt B), 198–205. https://doi.org/10.1016/j.ijdevneu.2015.09.004

Murtagh, F., & Legendre, P. (2014). Ward's hierarchical agglomerative clustering method: Which algorithms implement Ward's criterion? *Journal of Classification*, *31*(3), 274–295. https://doi.org/10.1007/s00357-014-9161-z

Nagelhus, E. A., Mathiisen, T. M., & Ottersen, O. P. (2004). Aquaporin-4 in the central nervous system: Cellular and subcellular distribution and coexpression with KIR4.1. *Neuroscience*, *129*(4), 905–913. https://www.sciencedirect.com/science/article/abs/pii/S0306452204007559?via%3Dihub

Namba, T., Mochizuki, H., Onodera, M., Mizuno, Y., Namiki, H., & Seki, T. (2005). The fate of neural progenitor cells expressing astrocytic and radial glial markers in the postnatal rat dentate gyrus. *European Journal of Neuroscience*, *22*(8), 1928–1941. https://doi.org/10.1111/j.1460-9568.2005.04396.x

Nielsen, S., Nagelhus, E. A., Amiry-Moghaddam, M., Bourque, C., Agre, P., & Ottersen, O. P. (1997). Specialized membrane domains for water transport in glial cells: High-resolution immunogold cytochemistry of aquaporin-4 in rat brain. *Journal of Neuroscience*, *17*(1), 171–180. https://www.jneurosci.org/content/17/1/171.long

Nixdorf-Bergweiler, B. E., Albrecht, D., & Heinemann, U. (1994). Developmental changes in the number, size, and orientation of GFAP-positive cells in the CA1 region of rat hippocampus. *Glia*, *12*(3), 180–195. https://doi.org/10.1002/glia.440120304

Norenberg, M. D. (1979). Distribution of glutamine synthetase in the rat central nervous system. *Journal of Histochemistry and Cytochemistry*, *27*(3), 756–762. https://journals.sagepub.com/doi/10.1177/27.3.39099

Oberheim, N. A., Goldman, S. A., & Nedergaard, M. (2012). Heterogeneity of astrocytic form and function. *Methods in Molecular Biology (Methods and Protocols)*, Milner R. (eds) Astrocytes., (Vol. *814*, pp. 23–45). Humana Press. https://doi.org/10.1007/978-1-61779-452-0_3

Oberheim, N. A., Takano, T., Han, X., He, W., Lin, J. H. C., Wang, F., Xu, Q., Wyatt, J. D., Pilcher, W., Ojemann, J. G., Ransom, B. R., Goldman, S. A., & Nedergaard, M. (2009). Uniquely hominid features of adult human astrocytes. *Journal of Neuroscience*, *29*(10), 3276–3287. https://doi.org/10.1523/JNEUROSCI.4707-08.2009

Oikonomidis, L., Santangelo, A. M., Shiba, Y., Clarke, F. H., Robbins, T. W., & Roberts, A. C. (2017). A dimensional approach to modeling symptoms of neuropsychiatric disorders in the marmoset monkey. *Developmental Neurobiology*, *77*(3), 328–353. https://doi.org/10.1002/dneu.22446

Park, J. E., Zhang, X. F., Choi, S. H., Okahara, J., Sasaki, E., & Silva, A. C. (2016). Generation of transgenic marmosets expressing genetically encoded calcium indicators. *Scientific Reports*, *6*, 34931. https://doi.org/10.1038/srep34931

Pignataro, D., Sucunza, D., Rico, A. J., Dopeso-Reyes, I. G., Roda, E., Rodríguez-Perez, A. I., Labandeira-Garcia, J. L., Broccoli, V., Kato, S., Kobayashi, K., & Lanciego, J. L. (2018). Gene therapy approaches in the non-human primate model of Parkinson's disease. *Journal of Neural Transmission*, *125*(3), 575–589. https://link.springer.com/article/10.1007%2Fs00702-017-1681-3

Poblete-Naredo, I., Guillem, A. M., Juárez, C., Zepeda, R. C., Ramírez, L., Caba, M., Hernández-Kelly, L. C., Aguilera, J., López-Bayghen, E., & Ortega, A. (2011). Brain-derived neurotrophic factor and its receptors in Bergmann glia cells. *Neurochemistry International*, *59*(8), 1133–1144. https://doi.org/10.1016/j.neuint.2011.10.002

Quesseveur, G., Fouquier d' Herouel A. F., Murai, K. K., & Bouvier, D. S. (2019). A specialized method to resolve fine 3D features of astrocytes in Nonhuman Primate (Marmoset, *Callithrix jacchus*) and human fixed brain samples. In B. Di Benedetto (Ed.), *Astrocytes. Methods in molecular biology* (Vol. *1938*). Humana Press. https://doi.org/10.1007/978-1-4939-9068-9. https://link.springer.com/protocol/10.1007%2F978-1-4939-9068-9_6. https://pubmed.ncbi.nlm.nih.gov/30617974/.

Rachev, S. T., Klebanov, L., Stoyanov, S. V., & Fabozzi, F. (2013). *The methods of distances in the theory of probability and statistics*. Springer Science & Business Media.

Raponi, E., Agenes, F., Delphin, C., Assard, N., Baudier, J., Legraverend, C., & Deloulme, J. C. (2007). S100B expression defines a state in which GFAP-expressing cells lose their neural stem cell potential and acquire a more mature developmental stage. *Glia*, *55*(2), 165–177. https://doi.org/10.1002/glia.20445

Regan, M. R., Huang, Y. H., Kim, Y. S., Dykes-Hoberg, M. I., Jin, L., Watkins, A. M., Bergles, D. E., & Rothstein, J. D. (2007). Variations in promoter activity reveal a differential expression and physiology of glutamate transporters by glia in the developing and mature CNS. *Journal of Neuroscience*, *27*(25), 6607–6619. https://doi.org/10.1523/JNEUROSCI.0790-07.2007

Reichenbach, A., & Wolburg, H. (2005). Astrocytes and ependymal glia. *Neuroglia*, *2*, 19–35. Oxford University Press. https://oxfordmedicine.com/view/10.1093/acprof:oso/9780195152227.001.0001/acprof-9780195152227-chapter-2

Roberts, A. C., Tomic, D. L., Parkinson, C. H., Roeling, T. A., Cutter, D. J., Robbins, T. W., & Everitt, B. J. (2007). Forebrain connectivity of the prefrontal cortex in the marmoset monkey (*Callithrix jacchus*): An anterograde and retrograde tract-tracing study. *Journal of Comparative Neurology*, *502*(1), 86–112. https://doi.org/10.1002/cne.21300

Rose, C. F., Verkhratsky, A., & Parpura, V. (2013). Astrocyte glutamine synthetase: Pivotal in health and disease. *Biochemical Society Transactions*, *41*(6), 1518–1524. https://portlandpress.com/biochemsoctrans/article-abstract/41/6/1518/68113/Astrocyte-glutamine-synthetase-pivotal-in-health?redirectedFrom=fulltext

Ross, C. N., Davis, K., Dobek, G., & Tardif, S. D. (2012). Aging phenotypes of common marmosets (*Callithrix jacchus*). *Journal of Aging Research*, *2012*, 567143. https://doi.org/10.1155/2012/567143

Rothstein, J. D., Martin, L., Levey, A. I., Dykes-Hoberg, M., Jin, L., Wu, D., Nash, N., & Kuncl, R. W. (1994). Localization of neuronal and glial glutamate transporters. *Neuron*, *13*(3), 713–725. https://doi.org/10.1016/0896-6273(94)90038-8

Rousseeuw, P. J. (1987). Silhouettes: A graphical aid to the interpretation and validation of cluster analysis. *Journal of Computational and Applied Mathematics*, *20*, 53–65. https://doi.org/10.1016/0377-0427(87)90125-7

Saab, A. S., Neumeyer, A., Jahn, H. M., Cupido, A., Simek, A. A. M., Boele, H.-J., Scheller, A., Le Meur, K., Gotz, M., Monyer, H., Sprengel, R., Rubio, M. E., Deitmer, J. W., De Zeeuw, C. I., & Kirchhoff, F. (2012). Bergmann glial AMPA receptors are required for fine motor coordination. *Science*, *337*(6095), 749–753. https://doi.org/10.1126/science.1221140

Santello, M., Toni, N., & Volterra, A. (2019). Astrocyte function from information processing to cognition and cognitive impairment. *Nature Neuroscience*, *22*(2), 154–166. https://doi.org/10.1038/s41593-018-0325-8

Sasaki, E., Suemizu, H., Shimada, A., Hanazawa, K., Oiwa, R., Kamioka, M., Tomioka, I., Sotomaru, Y., Hirakawa, R., Eto, T., Shiozawa, S., Maeda, T., Ito, M., Ito, R., Kito, C., Yagihashi, C., Kawai, K., Miyoshi, H., Tanioka, Y., … Nomura, T. (2009). Generation of transgenic non-human primates with germline transmission. *Nature*, *459*(7246), 523–527. https://www.nature.com/articles/nature08090

Sato, K., Oiwa, R., Kumita, W., Henry, R., Sakuma, T., Ito, R., Nozu, R., Inoue, T., Katano, I., Sato, K., Okahara, N., Okahara, J., Shimizu, Y., Yamamoto, M., Hanazawa, K., Kawakami, T., Kametani, Y., Suzuki, R., Takahashi, T., … Sasaki, E. (2016). Generation of a nonhuman primate model of severe combined immunodeficiency using highly efficient genome editing. *Cell Stem Cell*, *19*(1), 127–138. https://www.cell.com/cell-stem-cell/fulltext/S1934-5909(16)30153-9?_returnURL=https%3A%2F%2Flinkinghub.elsevier.com%2Fretrieve%2Fpii%2FS1934590916301539%3Fshowall%3Dtrue

Scharfman, H. E., & Binder, D. K. (2013). Aquaporin-4 water channels and synaptic plasticity in the hippocampus. *Neurochemistry International*, *63*(7), 702–711. https://doi.org/10.1016/j.neuint.2013.05.003

Shimogori, T., Abe, A., Go, Y., Hashikawa, T., Kishi, N., Kikuchi, S. S., Kita, Y., Niimi, K., Nishibe, H., Okuno, M., Saga, K., Sakurai, M., Sato, M., Serizawa, T., Suzuki, S., Takahashi, E., Tanaka, M., Tatsumoto, S., Toki, M., … Okano, H. (2018). Digital gene atlas of neonate common marmoset brain. *Neuroscience Research*, *128*, 1–13. https://doi.org/10.1016/j.neures.2017.10.009

Shinohara, Y., Konno, A., Takahashi, N., Matsuzaki, Y., Kishi, S., & Hirai, H. (2016). Viral vector-based dissection of marmoset GFAP promoter in mouse and marmoset brains. *PLoS ONE*, *11*(8), e0162023. https://doi.org/10.1371/journal.pone.0162023

Simard, M., & Nedergaard, M. (2004). The neurobiology of glia in the context of water and ion homeostasis. *Neuroscience*, *129*(4), 877–896. https://doi.org/10.1016/j.neuroscience.2004.09.053

Singh, A., & Abraham, W. C. (2017). Astrocytes and synaptic plasticity in health and disease. *Experimental Brain Research*, *235*(6), 1645–1655. https://doi.org/10.1007/s00221-017-4928-1

Skucas, V. A., Mathews, I. B., Yang, J., Cheng, Q., Treister, A., Duffy, A. M., Verkman, A. S., Hempstead, B. L., Wood, M. A., Binder, D. K., & Scharfman, H. E. (2011). Impairment of select forms of spatial memory and neurotrophin-dependent synaptic plasticity by deletion of glial aquaporin-4. *Journal of Neuroscience*, *31*(17), 6392–6397. https://doi.org/10.1523/JNEUROSCI.6249-10.2011

Steiner, J., Bernstein, H.-G., Bielau, H., Berndt, A., Brisch, R., Mawrin, C., Keilhoff, G., & Bogerts, B. (2007). Evidence for a wide extra-astrocytic distribution of S100B in human brain. *BMC Neuroscience*, *8*, 2. https://bmcneurosci.biomedcentral.com/articles/10.1186/1471-2202-8-2

Sun, W., Cornwell, A., Li, J., Peng, S., Osorio, M. J., Aalling, N., Wang, S., Benraiss, A., Lou, N., Goldman, S. A., & Nedergaard, M. (2017). SOX9 is an astrocyte-specific nuclear marker in the adult brain outside the neurogenic regions. *Journal of Neuroscience*, *37*(17), 4493–4507. https://www.jneurosci.org/content/37/17/4493.long

Takumi, T., Ishii, T., Horio, Y., Morishige, K., Takahashi, N., Yamada, M., Yamashita, T., Kiyama, H., Sohmiya, K., Nakanishi, S., & Kurachi, Y. (1995). A novel ATP-dependent inward rectifier potassium channel expressed predominantly in glial cells. *Journal of Biological Chemistry*, *270*(27), 16339–16346. https://www.jbc.org/article/S0021-9258(17)48868-5/fulltext

Tardif, S. D. (2019). Marmosets as a translational aging model-Introduction. *American Journal of Primatology*, *81*(2), e22912. https://doi.org/10.1002/ajp.22912

van Luijn, M. M., van Meurs, M., Stoop, M. P., Verbraak, E., Wierenga-Wolf, A. F., Melief, M.-J., Kreft, K. L., Verdijk, R. M., 't Hart, B. A., Luider, T. M., Laman, J. D., & Hintzen, R. Q. (2016). Elevated expression of the cerebrospinal fluid disease markers chromogranin A and clusterin in astrocytes of multiple sclerosis white matter lesions. *Journal of Neuropathology and Experimental Neurology*, *75*(1), 86–98. https://academic.oup.com/jnen/article/75/1/86/1851239

VanderVeen, N., Paran, C., Appelhans, A., Krasinkiewicz, J., Lemons, R., Appelman, H., Doherty, R., Palmer, D., Ng, P., Lowenstein, P. R., & Castro, M. G. (2014). Marmosets as a preclinical model for testing "off-label" use of doxycycline to turn on Flt3L expression from high-capacity adenovirus vectors. *Molecular Therapy Methods & Clinical Development*, *1*, 10. https://doi.org/10.1038/mtm.2013.10

Wang, F., Xu, Q., Wang, W., Takano, T., & Nedergaard, M. (2012). Bergmann glia modulate cerebellar Purkinje cell bistability via Ca2+-dependent K+ uptake. *Proceedings of the National Academy of Sciences of the United States of America*, *109*(20), 7911–7916. https://www.pnas.org/content/109/20/7911.long

Williams, S. M., Sullivan, R. K. P., Scott, H. L., Finkelstein, D. I., Colditz, P. B., Lingwood, B. E., Dodd, P. R., & Pow, D. V. (2005). Glial glutamate transporter expression patterns in brains from multiple mammalian species. *Glia*, *49*(4), 520–541. https://doi.org/10.1002/glia.20139

Yamamoto, M., Takeya, M., Ikeshima-Kataoka, H., Yasui, M., Kawasaki, Y., Shiraishi, M., Majima, E., Shiraishi, S., Uezono, Y., Sasaki, M., & Eto, K. (2012). Increased expression of aquaporin-4 with methylmercury exposure in the brain of the common marmoset. *Journal of Toxicological Sciences*, *37*(4), 749–763. https://www.jstage.jst.go.jp/article/jts/37/4/37_749/_article

Yang, J., Lunde, L. K., Nuntagij, P., Oguchi, T., Camassa, L. M. A., Nilsson, L. N. G., Lannfelt, L., Xu, Y., Amiry-Moghaddam, M., Ottersen, O. P.,

& Torp, R. (2011). Loss of astrocyte polarization in the tg-ArcSwe mouse model of Alzheimer's disease. *Journal of Alzheimer's Disease*, *27*(4), 711–722. https://content.iospress.com/articles/journal-of-alzheimers-disease/jad110725

Yang, Z., & Wang, K. K. (2015). Glial fibrillary acidic protein: From intermediate filament assembly and gliosis to neurobiomarker. *Trends in Neurosciences*, *38*(6), 364–374. https://doi.org/10.1016/j.tins.2015.04.003

Yuasa, S., Nakamura, K., & Kohsaka, S. (2010). *Stereotaxic atlas of the marmoset brain* (Vol. *1*). National Institute of Neuroscience, National Center of Neurology and Psychiatry. https://www.ncbi.nlm.nih.gov/books/NBK55612/

Zeng, X-N., Sun, X-L., Gao, L., Fan, Y., Ding, J-H., & Hu, G. (2007). Aquaporin-4 deficiency down-regulates glutamate uptake and GLT-1 expression in astrocytes. *Molecular and Cellular Neurosciences*, *34*(1), 34–39. https://www.sciencedirect.com/science/article/abs/pii/S1044743106002107?via%3Dihub

Zhang, Y., & Barres, B. A. (2010). Astrocyte heterogeneity: An underappreciated topic in neurobiology. *Current Opinion in Neurobiology*, *20*(5), 588–594. https://doi.org/10.1016/j.conb.2010.06.005

Zhao, H., Jiang, Y. H., & Zhang, Y. Q. (2018). Modeling autism in non-human primates: Opportunities and challenges. *Autism Research*, *11*(5), 686–694. https://doi.org/10.1002/aur.1945

SUPPORTING INFORMATION

Additional supporting information may be found in the online version of the article at the publisher's website.

FIGURE S1 Comparison of astrocytic markers in cortex using two different fixation methods. The fixation methods assessed were 10% formaldehyde (left panel) and 4% formaldehyde (right panel). Details about fixation methods can be found in the Material and Methods section. (A), GFAP labeling was used to identify different cortical astrocytes such as interlaminar astrocyte (ILA), protoplasmic, fibrous astrocyte and the endfoot compartment. Orange arrowheads indicate interlaminar astrocytic process and Roman numerals at the left side of the panel indicate approximate location of cortical layers. DAPI (blue) is used as a nuclear marker and AQP4 (blue) as an endfoot marker. Scale bars: 20 μm and 5 μm (endfoot). Pial ILA (B–E) and subpial ILA (F–I) astrocytes labeled by S100β (B, F), GS (C, G), Sox9 (D, H), and Kir4.1 (E, I). Yellow arrowheads show astrocytic soma and processes in B–I. Scale bar: 20 μm. bv, blood vessel

FIGURE S2 Comparison of astrocytic markers in hippocampus using two different fixation methods. The fixation methods assessed were 10% formaldehyde (left panels) and 4% formaldehyde (right panel). Details about fixation methods can be found in the Material and Methods section. Hippocampal astrocytes were labeled with the astrocytic markers: GS (A), Sox9 (B), and GFAP (C). Double immunostaining of GS and SOX9 (D), GS and GFAP (E), and S100β and GFAP (F) to show heterogeneous expression. Scale bar: 50 μm. (G), GFAP labeling was used to identify polarization of astrocytes located at the edge of pyramidal layer (apical processes (a), basal processes (b)) and astrocytes in S. radiatum (H). Scale bar: 20 μm. Astrocytic markers (EAAT2, GAT3, and AQP4) were also display in gray scale (I) and in heat maps (J) showing the density of expression of each marker. A purple–blue color indicates lower intensity signal and red–yellow color means higher intensity signal. White arrows highlight areas of particularly high signal intensity. Scale bars: 50 μm

FIGURE S3 Comparison of astrocytic markers in cerebellum using two different fixation methods. The fixation methods used were 10% formaldehyde (left panel) and 4% formaldehyde (right panel). Details about fixation methods can be found in the Material and Methods section. Coronal sections were labeled using GFAP (A), S100β (B), GS (C) and Sox9 (D). Lower magnification images show four different areas: molecular layer (ML), Purkinje cell layer (PCL), granule cell layer (GCL), and white matter (WM). DAPI was used to identify nuclei (blue staining). Scale bars: 100 μm. Second and right panels show higher magnification of Bergmann glia (BG), velate astrocytes (VA), and astrocytes located in WM. In BG images, white asterisks indicate Purkinje cell bodies and white arrows show lateral BG processes. White arrowheads indicate astrocytic soma in VA and WM. Scale bars: 50 μm (BG) and 20 μm (VA, WM). Astrocytic markers such as GluA1, Kir4.1, EAAT2, AQP4, and Cx43 were also used in lower magnification images (E) and higher magnification of ML and GCL (F). Purkinje cell bodies are indicated with a white asterisk. Scale bar: 100 μm (E) and 20 μm (F)

FIGURE S4 Agglomerative indices for images analyzed. High values reflect tight clustering of objects, whilst low values indicate weaker-formed clusters. Note that Ward2 criteria were among the best options for clustering

FIGURE S5 Cortical heterogeneity of GS immunolabeling. Left, dendrogram showing astrocytic clusters assigned by the hierarchical clustering algorithm. Right, spatial organization of clusters. GS expression was used to identify individual astrocytes and they were assigned in a region from pia matter surface (R1) to inner cortical layer (R2, R3, and R4). Scale bars: 50 μm. Each astrocyte was identified with a number. Each cluster was identified with a number and particular color and the percentage of each cluster in regions 1–4 is shown in a′. A more detailed description can be found in the legend for Figure 4

FIGURE S6 Heterogeneity of EAAT2, GAT3, and GS immunolabeling in hippocampus. Left, dendrogram showing astrocytic clusters assigned by hierarchical clustering algorithm for EAAT2 (A), GAT3 (B), and GS (C). (a–c) show the spatial organization of cells within clusters. GS expression was used to identify individual astrocytes. Astrocyte were assigned to the S. radiatum, S. pyramidale, and S. oriens and were assigned a number. Scale bars: 50 μm. Each cluster was identified with a number and a particular color and the percentage of each cluster into S. oriens, S. pyramidale, and S. radiatum is shown in a′–c′. A more detailed description can be found in the legend for Figure 7

Transparent Science Questionnaire for Authors

Transparent Peer Review Report

How to cite this article: Muñoz, Y., Cuevas-Pacheco, F., Quesseveur, G., & Murai, K. K. (2021). Light microscopic and heterogeneity analysis of astrocytes in the common marmoset brain. *Journal of Neuroscience Research*, 99, 3121–3147. https://doi.org/10.1002/jnr.24967